PERGAMON

Pattern Recognition 36 (2003) 2967–2991

PATTERN RECOGNITION
THE JOURNAL OF THE PATTERN RECOGNITION SOCIETY

www.elsevier.com/locate/patcog

Computer-aided detection and classification of microcalcifications in mammograms: a survey

H.D. Cheng*, Xiaopeng Cai, Xiaowei Chen, Liming Hu, Xueling Lou

Department of Computer Science, Utah State University, Logan, UT 84322-4205, USA

Received 11 March 2003; accepted 7 May 2003

Abstract

Breast cancer continues to be a significant public health problem in the world. Approximately, 182,000 new cases of breast cancer are diagnosed and 46,000 women die of breast cancer each year in the United States. Even more disturbing is the fact that one out of eight women in US will develop breast cancer at some point during her lifetime. Primary prevention seems impossible since the causes of this disease still remain unknown. Early detection is the key to improving breast cancer prognosis. Mammography is one of the reliable methods for early detection of breast carcinomas. There are some limitations of human observers, and it is difficult for radiologists to provide both accurate and uniform evaluation for the enormous number of mammograms generated in widespread screening. The presence of microcalcification clusters (MCCs) is an important sign for the detection of early breast carcinoma. An early sign of 30–50% of breast cancer detected mammographically is the appearance of clusters of fine, granular microcalcification, and 60–80% of breast carcinomas reveal MCCs upon histological examinations. The high correlation between the appearance of the microcalcification clusters and the diseases show that the CAD (computer aided diagnosis) systems for automated detection/classification of MCCs will be very useful and helpful for breast cancer control. In this survey paper, we summarize and compare the methods used in various stages of the computer-aided detection systems (CAD). In particular, the enhancement and segmentation algorithms, mammographic features, classifiers and their performances are studied and compared. Remaining challenges and future research directions are also discussed.

Keywords: Microcalcifications; Mammography; Computer-aided detection; Contrast enhancement; Segmentation; Features extraction; Microcalcification clusters (MCCs) detection and classification; False positive (FP); False negative (FN); Receiver operating characteristic (ROC); Free-response receiver operating characteristic (FROC)

1. Introduction

Breast cancer continues to be a significant public health problem in the world. Approximately, 182,000 new cases of breast cancer are diagnosed and 46,000 women die of breast cancer each year in US. Even more disturbing is the fact that one out of eight women in US will develop breast cancer at some point during her lifetime [1,2]. Primary prevention seems impossible since the causes of this disease still remain unknown. Early detection is the key to improving breast cancer prognosis. The earlier the cancer is detected, the better a proper treatment can be provided. For women whose tumors were discovered early by mammogram the five year survival rate was about 82% as opposed 60% that not been found early [1]. Mammography is one of the most reliable methods for early detection of breast carcinomas. However, it is difficult for radiologists to provide both accurate and uniform evaluation for the enormous number of mammograms generated in widespread screening. There are some limitations of human observers: 10–30% of breast lesions are missed during routine screening. With the advances of digital image processing, pattern recognition and artificial intelligence,

* Corresponding author. Tel.: +1-435-797-2054; fax: +1-435-797-3265.

E-mail address: cheng@hengda.cs.usu.edu (H.D. Cheng).

0031-3203/$30.00
doi:10.1016/S0031-3203(03)00192-4

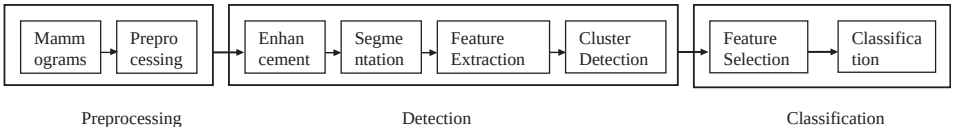

Fig. 1. Block diagram of mammography CAD system.

radiologists have an opportunity to improve their diagnosis with the aid of computer systems [3–15]. On average, the readers' sensitivity can be increased by 10% with the assistance of CAD (computer aided diagnosis) systems [16]. The presence of microcalcification clusters (MCCs) is an important sign for the detection of early breast carcinoma. An early sign of 30–50% of breast cancer detected mammographically is the appearance of clusters of fine, granular microcalcification [2,3,17,18], and 60–80% of breast carcinomas reveal MCCs upon histological examinations [19]. The high correlation between the appearance of the microcalcification clusters and the diseases show that the automated detection/classification of MCCs can be very helpful for breast cancer control. Although computer-aided mammography has been studied over two decades, automated interpretation of microcalcifications remains very difficult. It is mainly due to their fuzzy nature, low contrast and low distinguishability from their surroundings:

(1) Microcalcifications are very small. The sizes of microcalcifications are in the range of 0.1–1.0 mm, and the average is about 0.3 mm. Some isolated ones smaller than 0.1 mm cannot be distinguished in the film-screen mammography from the high-frequency noise.
(2) Microcalcifications with various sizes, shapes, and distributions, therefore, simple template matching is impossible.
(3) Microcalcifications may be low contrast so that the intensity difference between suspicious areas and their surrounding tissues can be quite slim.
(4) Microcalcifications may be closely connected to surrounding tissues, and simple segmentation algorithms cannot work well.
(5) In some dense tissues, and/or skin thickening, especially in the breasts of younger women, suspicious areas are almost invisible. The dense tissues especially in younger women may easily be misinterpreted as microcalcifications, and a high false-positive (FP) rate, that is the major problem with most of the algorithms, will be yielded. Most of FPs are due to film emulsion error, digitization artifacts, or anatomical structures such as fibrous strands, breast borders, or hypertrophied lobules that look like microcalcifications.

To deal with the above problems, it is very important to suppress the noise, to enhance the contrast between the region of interest (ROI) and background, to extract and select the features of microcalcifications effectively, and hence, to detect/classify microcalcifications more accurately. There are many approaches for enhancement of microcalcification clusters, including various filtering methods, global and local thresholding methods, histogram equalization, mathematical morphology transformations, statistic methods, wavelet transformations, multiresolution processing approaches, neural networks, stochastic models, fractal models, high-order statistic methods, fuzzy logic approaches, etc. A typical computer-aided mammography screening system can be described by the block diagram in Fig. 1. Usually, the preprocessing block includes digitization of the mammograms with different sampling and quantization rates. Then, the regions of interests selected from the digitized mammogram are de-noised and enhanced. The segmentation block is designed to find suspicious areas containing MCCs, and to separate the MCCs from the background that will be used for extracting features of MCCs. In the feature extraction and selection block, the features of MCCs will be extracted and selected, and MCCs will be classified into benign, malignant and normal.

2. Enhancement of microcalcifications

The contrast enhancement methods can be categorized as indirect and direct approaches. Indirect approaches, mainly, modify the histograms without defining the contrast. Direct approaches define the contrast first, then enhance the contrast based on the defined measurements. We can also categorize contrast enhancement algorithms according to if they will use global information, local information or both global and local information. The major problem with the contrast enhancement algorithms is that for an image, some regions may be under-enhanced while some regions may be over-enhanced. Under-enhancement can cause false negatives (FNs), and over-enhancement can cause false positive (FPs).

Mainly, image enhancement includes intensity and contrast manipulation, noise reduction, background removal, edges sharpening, filtering, etc. The task of mammogram enhancement is to sharpen the edges or boundaries of ROIs, or to increase the contrast between ROIs and background [20]. It is well-known that if a region differs in luminance from its surroundings by less than 2%, it is indistinguishable to human eye [21]. Although microcalcifications usually are brighter than their surroundings, the contrast for some

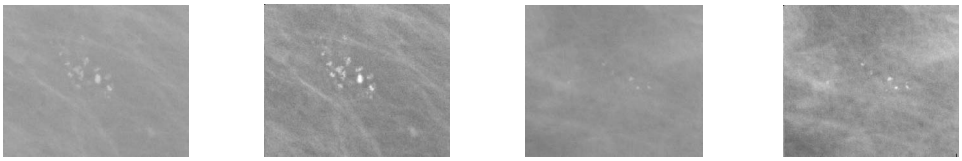

(a) (b) (c) (d)

Fig. 2. (a) Original mammogram, (b) enhanced image of (a), (c) Original mammogram, (d) enhanced image of (c).

microcalcifications in a dense breast is quite low that human eyes can hardly distinguish them. The aim of contrast enhancement is to increase the contrast of microcalcifications over the threshold. Fig. 2 displays some digital mammograms and the corresponding enhanced images [22]. In this section, we summarize the enhancement techniques and discuss some measurements for evaluating the performance of the enhancement algorithms.

2.1. Conventional enhancement techniques

Conventional enhancement techniques mainly are the global and fix-neighborhood techniques that may adapt to the global features or local features within a fix neighborhood, and they modify the images based only on global properties. The contract stretching techniques, histogram equalization, unsharp masking, spatial filtering are the major techniques. Microcalcifications vary greatly in sizes and shapes, and the contrast between the ROIs and the surrounding tissues is varying greatly, therefore, mammograms cannot be enhanced by the global or fix-neighborhood techniques due to their lack of adaptiveness. Most of the conventional enhancement techniques enhanced not only the microcalcifications but also the background and noise. It will have the under-enhancement and over-enhancement problems, i.e., some regions are underenhanced while some regions are overenhanced.

2.1.1. Contrast stretching

Contrast stretching is the simplest enhancement method. Typically, it is employed when the gray-level distribution is narrow. The method is to adjust the histogram to achieve a greater separation between the foreground and background gray-level distributions. The simplest transformation is the linear rescaling transformation

$$f(x) = kx + m, \tag{1}$$

where x is the input image gray scale value and $f(x)$ is the transformed gray scale value, k and m are constants. It is easy to see that all the values increase at the same rate. Alternatively, a nonlinear transformation is used

$$f(x) = kx^p \tag{2}$$

and a more general transformation is

$$f(x) = \begin{cases} f_1(x), 0 \leqslant x < s_1, \\ f_2(x), s_1 \leqslant x < s_2, \\ \quad\vdots \\ f_n(x), s_{n-1} \leqslant x \leqslant L, \end{cases} \quad \begin{array}{l} L \text{ is the maximum gray} \\ \text{value of the original image.} \end{array} \tag{3}$$

Although these transforms can remove the uniform background, it is difficult to reduce the noises whose gray levels are similar to that of the microcalcifications.

2.1.2. Enhancement by histogram equalization method

Considering the histogram of a mammogram as a probability distribution, base on information theory, the mammogram with a uniform histogram will have more information. We can get the maximum entropy if we equalize the histogram as uniform as possible, and it results in the enhancement of mammograms. In order to equalize the histogram independently in segmental regions, adaptive histogram equalization method can be used [23]. However, some normal tissues and noise will still be enhanced.

2.1.3. Convolution mask enhancement

Convolutional masking is commonly used for mammography enhancement. The unsharp masking [24,25] and Sobel gradient operators are two examples. The unsharp masking can be expressed as [25]

$$D_p(x, y) = D_o(x, y) + K(x, y) \times \left[D_o(x, y) - \frac{1}{mn} \sum_{j=1}^{n} \sum_{i=1}^{m} D_o(x_i, y_j) \right], \tag{4}$$

where $D_0(x, y)$ and $D_p(x, y)$ are the densities of the original and the processed mammograms, respectively. The last term is the unsharp term with an $m \times n$ area centered at pixel (x, y). $K(x, y)$ is a weight factor. The mask size and the weight factor determine the frequency range and the degree of enhancement. The unsharp masking method reduces the low-frequency information while amplified the high-frequency detail. However, these processes could change the images dramatically to be applied to the mammograms.

2.1.4. Fixed and adaptive neighborhood enhancement

Though there are some modifications of the above techniques based on local properties, they are still lack of the adaptiveness to the local information. For some mammograms with inhomogeneous background, the local-based enhancement method can be more useful. Local enhancement techniques use statistical properties such as the local mean and the local standard deviation in a fixed neighborhood of the pixel to estimate the background, and to suppress it to increase the local contrast [26]. Gordon and Rangayyan [27] used fixed neighborhood method to enhance the mammogram. But the square-root function used in the algorithm enhanced the noise and other background variations as well that it is difficult to distinguish the microcalcifications from the enhanced noise and background. Furthermore, the contrast-ratio adaptive neighborhood process also resulted in the loss of some microcalcification features, hence, both the false positive rate and false negative rate are high. Dhawan et al. [28] used an optimal adaptive enhancement method to reduce the influence. One of the requirements of the contrast enhancement function is to provide $40–50^{\circ}$ slope in the low input range $(0–0.1)$ to reduce noise enhancement. Four contrast enhancement functions were studied: the square root function $(\sqrt{\Gamma})$, the exponential $(1 - e^{-k\Gamma})$, the logarithm $(\ln(1 + k\Gamma)$, and the trigonometric $(\sin(k\Gamma), \tan(k\Gamma), \tanh(k\Gamma))$ where Γ is the local contrast. For each function $F(k\Gamma)$, k was selected to satisfy the requirement $|dF(k\Gamma)/d\Gamma|_{\Gamma=0}^{\Gamma=0.1} = 1$.

2.2. Region-based enhancement

Region-based image processing technique has been applied to segmentation and contrast enhancement [29–33]. Here, we only focus on its application to contrast enhancement. Region-based approach enhances the contrast of the mammographic features of ROIs with various sizes and shapes according to the change of their surroundings. The extent and shape of the grown region adapt to local variation of the gray levels. Contrast is computed with respect to its background. The definition of extent of regions is critical for region-based process. Usually there are two classes of regions: nonoverlapping regions, which are obtained by image segmentation technique, and overlapping regions, which are achieved by the region growing techniques. Overlapping regions were employed to avoid noticeable edge artifacts and an inferior enhanced mammogram [29]. Region-based method can enhance more anatomical detail without significantly introducing artifacts, and has demonstrated that it can identify calcifications more effectively in the image of dense breasts where the contrast between calcifications and breast tissue is quite low [29].

2.3. Feature based enhancement

As mentioned above, the conventional enhancement techniques cannot be useful for enhancing microcalcification features. Recently, there were two approaches to enhance microcalcifications adapted to their features. One is to increase the contrast of suspicious areas [34–40], and another is to remove the background structures and noise according to microcalcification features [1,2,21,41–48].

The mammographic image was processed by a subband decomposition filterbank, and then the unoverlapping squares in the bandpass subimage used higher order statistical (HOS) parameters such as third-order correlation, skewness, and fourth-order correlation, kurtosis, etc., as the measures of the asymmetry and impulsiveness of the distribution to detect microcalcification clusters. If the values of skewness and kurtosis are distinctly greater than zero, it implies that the regions have microcalcifications. On the other hand, if they are very close to zero, it means that the areas have a gaussian-like distribution with no microcalcifications [34,35]. An enhancement technique using fuzzy set theory and geometrical statistics to increase the contrast of microcalcifications was studied [22,36,49]. Since mammograms have some degree of fuzziness such as indistinct borders, ill-defined shapes, and different densities, the original images are transformed into a fuzzified image according to the maximum fuzzy entropy principle, and then the geometrical statistics is used to measure the nonuniformity of the regions. In order to reduce the FP further, a curve detector is employed to remove those line-like or curve-like irrelevant breast structures. Multiscale analysis methods were also used to enhance the MCCs [36]. The methods of contrast enhancement are based on three multiscale representations: the dyadic wavelet transform, the φ-transform and the hexagonal wavelet transform. Mammograms are reconstructed from wavelet coefficients modified at one or more levels by local and global nonlinear operators [37]. An adaptive mammographic image enhancement using first derivative and local statistics was studied [38–40].

An alternative to contrast enhancement is the removal of background from foreground. Usually the resulting image can be obtained by subtracting a low-pass filtered version of the image from the original. In Refs. [1,2], the suppressed image is subtracted from the enhanced image to remove structure background. Mascio et al. [48] enhanced the image by the round high-emphasis technique which is a high-pass filter preserving round edges and texture gist which is the average of morphological opening and closing subtracted from the original image. In Refs. [41,42], a pattern-dependent enhancement algorithm based on the fractal modeling scheme was studied. Comparing with microcalcifications, the breast background tissues have high local self-similarity which is the basic property of fractal objects. A fractal modeling approach was used to analyze and model breast tissue background. Then, microcalcifications can be enhanced by employing the difference between the original image and the modeled image. Morphological processing [21,43] and wavelet reconstruction [44–48] are two other successful methods to estimate the background. They both

employed transforms to estimate the background according to the features and to remove the background.

2.4. Evaluation of enhancement algorithms

It is very difficult to measure the improvement of the enhancement objectively. If the enhanced image can make observer perceive the region of interest better, then we can say that the original image has been improved. In order to compare different enhancement algorithms, it is better to design some methods for the evaluation of enhancement objectively. The statistical measurements such as variance or entropy can always measure the local contrast enhancement, however, that show no consistency for the mammograms.

Morrow et al. [29] propose a measure of contrast histogram that is a graph of the distribution of contrast over image. The width of a contrast histogram can be quantified by the second moment,

$$M_2 = \sum_{i=1}^{N} c_i^2 \, p(c_i), \tag{5}$$

where c_i computed by using Eq. (7) are the contrast values falling in the ith bin of N bins, $p(c_i)$ is the normalized number of occurrences of the contrast c_i. A low-contrast image has a narrow contrast histogram, while a high-contrast image has a broader contrast histogram. The second moment M_2 for the enhanced image is bigger than that of the original image, and it indicates that the contrast spread is wider in the enhanced image.

Laine et al. [37] proposed the contrast improvement index (CII) as the measure of the enhancement performance:

$$CII = \frac{C_{processed}}{C_{original}}, \tag{6}$$

where $C_{processed}$ and $C_{original}$ are the contrasts for a ROI in the processed and original images, respectively. The contrast C of a region is defined by

$$C = \frac{f - b}{f + b}, \tag{7}$$

where f is the mean gray-level value of the foreground and b is the mean gray-level value of the background. The bigger value of CII, the better performance.

In Refs. [38–40] the measures of enhancement performance are the contrast improvement ratio (CIR) and the receiver operating-characteristics (ROC) analysis. The bigger CIR indicates the better performance of the enhancement. The local contrast $c(x, y)$ is adopted to define CIR [20]:

$$c(x, y) = \frac{|S(x, y) - \bar{E}(x, y)|}{S(x, y) + \bar{E}(x, y)}, \tag{8}$$

$$CIR = \frac{\sum_{(x,y)\in R} [c(x, y) - \tilde{c}(x, y)]^2}{\sum_{(x,y)\in R} c(x, y)^2}, \tag{9}$$

where $S(x, y)$ is the output of the film-artifact removal filtering and $\bar{E}(x, y)$ is the mean edge gray level. $c(x, y)$ and $\tilde{c}(x, y)$ are the local contrast values of the original image and the enhanced image, respectively.

Li et al. [41,42] used contrast, contrast improvement index (CII), background noise level, peak signal-to-noise ratio ($PSNR$), and average signal to noise ratio ($ASNR$) to evaluate the enhancement performance. The definitions of contrast and CII are the same as Eqs. (6) and (7) [37], and the background noise level is measured by the standard derivation σ of the background:

$$\sigma = \sqrt{\frac{1}{N} \sum_{i=1}^{N} (b_i - b)^2}, \tag{10}$$

where b_i is the gray-level value of a surrounding background region, and N is the total number of pixels in the surrounding background region.

$PSNR$ and $ASNR$ are defined as follows:

$$PSNR = \frac{p - b}{\sigma} \quad \text{and} \quad ASNR = \frac{f - b}{\sigma}, \tag{11}$$

where p is the maximum gray-level value of a foreground. The values of the two indexes larger, the enhancement performance better. In Table 1, we list some enhancement techniques with the evaluation measures. We add a column listing image resolutions, since the resolutions of the images will affect the results of the enhancement. Readers should notice that the evaluation of enhancement just like the evaluation of segmentation that it is still an open problem.

3. Segmentation of microcalcifications

In general, segmentation is to divide the image I into nonoverlapping regions S_i:

$$\bigcup S_i = I \quad \text{and} \quad S_i \cap S_j = \Phi, \; i \neq j.$$

Image segmentation deals with the extraction of objects from the background. When an object is in a uniform background, the histogram of the image will have two distinct peaks separated by a valley. If we choose a threshold T at the valley, then we can segment the image by letting

$$g = \begin{cases} L_{\min} & \text{if } g \leqslant T, \\ L_{\max} & \text{otherwise,} \end{cases}$$

where $L_{\min}$ and $L_{\max}$ are the minimum and maximum grey levels, respectively. However, due to the variations in shapes, sizes and intensities of microcalcifications, it is difficult to choose a threshold at the valley of the histogram which, in general, is not bimodal.

There are two different goals for the segmentation of microcalcifications [50]. One is to obtain the locations of suspicious areas to assist radiologists for diagnose. The other

Table 1
An overview of the enhancement techniques

Methods	Examples	Evaluation
Conventional enhancement techniques (global or fixed size window)	Unsharp masking [25]. The unsharp masking method reduces the low frequency information while amplified the high frequency detail. However these processes change the images too dramatically.	0.1 mm × 0.1 mm per pixel 10 bits/pixel. 12 images with MCCs and 12 normal images
	Optimal adaptive neighborhood image processing [28]. Four contrast enhancement functions were studied.	8 bits/pixel. Use the entropy as the measurement
	Adaptive mammography enhancement using the first derivative operators such as Sobel operators, the compass operations, and local statistics of a mammogram [38].	180 μm × 180 μm per pixel 12 bits/pixel. Contrast Improvement Ratio (CIR) and ROC analysis
Region-based enhancement	Region-based contrast enhancement uses each pixel as a seed to grow a region [29]. Contrast is enhanced by applying an empirical transformation based on each region's seed pixel value, its contrast, and its background.	Less than 0.1 mm square pixel size, 12 bits/pixel, 10 case images. Contract and Contrast histogram
Feature based enhancement	Multiscale analysis [37] based on the dyadic wavelet transform, the φ-transform, and the hexagonal wavelet transform.	200 μm × 200 μm per pixel 12 bits/pixel. Contrast Improvement Index (CII)
	Fractal approach compared with the partial wavelet reconstruction and the morphological operation approaches [41,42]. (1) The fractal and morphological approaches can remove more background structures than wavelet approach does, especially for those ROIs with very low contrast compared with the surrounding background. (2) The wavelet approach can preserve the overall shape of spots better than the fractal and morphological approaches.	0.1 mm × 0.1 mm per pixel, 12 bits/pixel, 30 mammogram images. (1) Contrast, (2) The CII, (3) Standard derivation σ, (4) PSNR, (5) ASNR

is to classify the abnormalities of the breast into benign or malignant. Local thresholding is used by setting threshold values for sub-images. It requires selection of a window size and threshold parameters. In Ref. [4], the threshold for a pixel is set as the mean value plus the RMS noise value multiplied by a selected coefficient in a selected square region around the thresholded pixel [5,51]. The threshold is based on an expected bimodal intensity distribution in a selected size window that contains the sub-image to be segmented. The original image is partitioned into square sub-images and any quarter of a sub-image is overlapped by four other sub-images (Fig. 3). Each grey level histogram of the sub-image is smoothed by a median filter to remove local maxima and minima. Then, the resulting histogram is classified as either bimodal or unimodal. A threshold is set at the valley of the histogram if the histogram is bimodal, otherwise, the threshold is set initially at the present maximum grey level. Once all sub-images have been processed, each unimodal threshold is replaced by a value interpolated from neighboring sub-images. For any pixel, it will have up to five separately determined thresholds. A threshold such as the average or the median of the five thresholds or the ith ($i = 1, 2, 3, 4, 5$) biggest threshold is chosen to decide if the pixel belongs to the normal background.

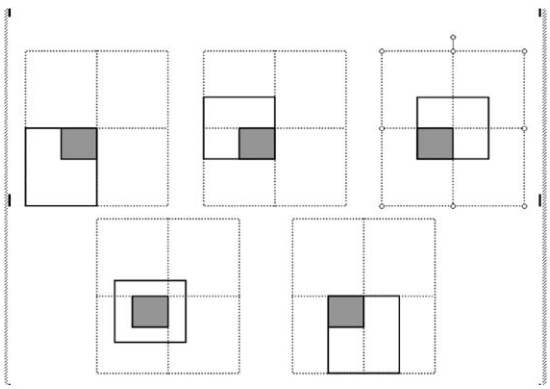

Fig. 3. Five sub-images used for local area thresholding (solid line) [51].

Region growing is a well-known method of segmentation. This method groups the pixels with the properties similar to these of a "seed" pixel. This method requires the specification of two variables: the window size and the absolute difference in gray levels between the processed pixel and the seed pixel. Once the growing region algorithm is terminated, if the average intensity of the grown region is much greater than the surrounding region, then the pixel is classified as a pixel of the microcalcification. Every pixel in the image is chosen successively as the seed pixel and the above procedure is repeated. Kallergi et al. [30] compared local thresholding and region growing methods. It showed that the local thresholding method has greater stability, but is more dependent on parameter selection. Woods et al. [31] used local thresholding by subtracting the average intensity of a 15×15 window from the processed pixel. Then, region growing is performed to group pixels into objects. Bankman et al. [52] developed a new segmentation algorithm without threshold or window selection or parametric data models. Comparing with the multi-tolerance region growing algorithm [32] and the active contour model [53], it showed that the speed of the algorithm is more than an order of magnitude faster than the other two.

Edge detection is a traditional method for segmentation. Many operators, Roberts gradient, Sobel gradient, Prewitt gradient and Laplacian operator, were published. Some mathematical morphological operations such as erosion, top-hat transformation and more complicated morphological filters with multi-structure elements can also be used [21,54–57]. It is good in dealing with geometrically analytic aspects of image analysis problems. When using multiscales and multistructuring elements, the results will not be affected by the complex background information and the extracted images are not distorted much. But morphological operation requires a priori knowledge of the resolution level of the mammograms in order to determine the sizes and shapes of the structure elements. Zhao et al. [56] developed a method to extract suspicious calcifications based on morphological adaptive threshold and morphological skeleton information. The threshold set is decided by the index numbers in the skeleton of shapes that represent calcifications. The parameters of the adaptive threshold sets were obtained from interpreting umbra shadows from an image function. The control parameter is based on the integer value extracted from a single layer of the skeleton transform as follows

$$SK(X) = \bigcup_{r>o} S_n(X),$$

$$= S_n(X)(X \Theta nB) - (X \Theta (n+1)B), \tag{12}$$

where X is the object and nB is the n dilations of structure element B, i.e., $nB = \underbrace{B \oplus B \oplus \cdots \oplus B}_{n}$ and $\oplus$ is the dilation operation. Θ denotes the erosion operation. The criterion for selecting the threshold value is that the skeleton should match with the size description of calcifications.

CAD also applies wavelet transform for feature enhancement, segmentation and classification [9,55,58–75]. The multiresolution wavelet representation provides a natural hierarchy to embed an interactive paradigm for accomplishing scale-space feature analysis. Similar to traditional coarse to fine matching strategies, the radiologist may first look at coarse features within a low frequency level of the wavelet transform and later examine finer features (e.g. microcalcifications) at a high frequency level. The common scheme for wavelet transform on the detection of microcalcification is to reconstruct the image from transform coefficients modified at each level by local and global nonlinear operators. Using the multiresolution capability, the wavelet transform could separate small objects (microcalcifications) from large objects (background structures). Yoshida et al. [60] showed that the resolution level 1 mainly included the high-frequency noise, whereas levels 2 and 3 enhanced microcalcifications effectively. Levels greater than 3 showed a large correlation with the nonuniform background. In order to obtain the maximum performance, two keys issues should be paid more attention: wavelet base and nonlinear functions of the wavelet coefficients. Tree-structure wavelet transform is also used to obtain better microcalcification segmentation [68,69,76]. Nonlinear multistage tree structured filter suppressed the noise and an quasi-range edge detection and wavelet transform completed the segmentation. The morphology of the segmented microcalcification and the spatial extent of the cluster were preserved well, which is important for the later classification. A list of different wavelets used for processing microcalcifications is given in Table 2.

Stochastic approaches have also been used to segment calcifications [23,65,78,81,82,92]. Stochastic and Bayesian methods have provided a general framework to model images and to express prior knowledge. Markov random field model was used to deal with the spatial relations between the labels obtained in an iterative segmentation process [23,78,81,82]. The process assigning pixel labels iteratively can be achieved by maximizing either a posteriori estimation or posterior marginal estimation. The pixel labels x_i are iteratively updated by maximizing their probabilities, given the image data in a small neighborhood y_{δ_i} of site i and given the current estimate of the rest of the labels $\hat{X}_{S\setminus i}$

$$x_i' = \max_l [p(x_i = l \mid y_{\delta_i}, \hat{X}_{S\setminus i})], \tag{13}$$

where l represents four pixel classes: background, microcalcifications, line/edge and film emulsion error. The image data y_{δ_i} is presented by three local image features: the two local contrasts at two different spatial resolutions and the output of a line/edge detector. The probability to be maximized can be written as

$$p(x_i = l \mid y_{\delta_i}, \hat{X}_{S\setminus i}) \propto f(\Theta_i \mid x_i = l, \hat{X}_{S\setminus i}) \cdot p(x_i = l \mid \hat{X}_{S\setminus i}), \tag{14}$$

Table 2
An overview of the segmentation methods

Segmentation technique and description	Advantages and disadvantages	References
Statistical method: Using global or local statistics such as histogram, mean, standard deviation, etc.	It does not need a prior information for the histogram thresholding of the image and can be used widely work very well with low computation complexity, but it do not work without peaks and sometimes the segmented region cannot be contiguous.	Histogram threshold-holding [4,5,30,31,50,51,55,77–80], MRF Method [23,54,65,81,82]
Region-based approach: Group pixel into homogeneous regions.	Works best when the region homogeneity criterion is easy to define. It depends on the selection of seed region and the termination conditions. It is expensive both in computational time and memory.	Region growing approach [32,57,83] Surrounding region dependence [39]
Mathematical morphology: Using morphological filters or transforms to get the edge or skeleton information to threshold the region.	It is good in dealing with geometric analytic aspects of image analysis problems. When using the multiscale and multistructuring elements, the results are not affected by the complex background and the extracted images are not distorted much. But it requires a priori knowledge of the resolution level of the mammograms in order to determine the sizes and shapes of the structure elements.	Top-hat [21,54,56] Erosion [55] Morphological filter with multiscale and multi elements [57]
Multiscale analysis: Design wavelet-based filters to transform the image from spatial domain to spatial frequency domain, and to perform further processing.	Due to its ability of discriminating different frequencies, the method can preserve the resolution of the portion of ROI. And it does not require the use of heuristics or a prior knowledge of the size and the resolution of the mammogram.	Multichannel wavelet transform [76,84,85] B-spline function [79] Multiresolution statistics analysis [86] Multiscale analysis [64,86,87] Decimated wavelet transform [47,60] Undecimated biorthogonal transform [61–64]
The fractal model: Image context can be modeled by fractal objects which are attractors of sets of 2-D affine transformations.	Mammograms possess structures with high local self-similarity which is the basic property of fractal object. But it consumes too much computation time.	Fractal model [41,42,50]
Fuzzy approaches: Apply fuzzy operators, property, inference rules to handle the uncertainty inherent in the image.	Due to variable shapes of microcalcifications, it is a good way to use fuzzy rules to perform approximate inference. But the determination of fuzzy membership is not easy.	Fuzzy logic [36,88–91]

where Θ_i is a vector with the values of the above three features at a particular site. The a priori probability $p(x_i = l \mid \hat{X}_{S\setminus i})$ of labels represents the Markov random field (MRF) and models the spatial relations.

The merit of MRF image modeling is that it provides a strong exploitation of the pixel correlations. The segmentation results can be further enhanced via the application of maximum a posteriori (MAP) segmentation estimation scheme based on the Bayesian learning paradigm [81,82].

4. Microcalcification detection

We will analyze different microcalcification detection approaches based on feature extraction methods.

The following feature sets are used:

- individual microcalcification features;
- statistical texture features;
- multi-scale texture features;
- fractal dimension features.

4.1. Template matching

Template matching is the simplest and earliest approach to pattern recognition. A template, typically, is a 2D pattern. The pattern to be recognized is matched against the stored templates. The bivariate Gaussian function is used to detect smaller microcalcifications and two dimension sech functions are used to detect bigger microcalcifications [93]. However, it only gave a simulation result and the test on mammograms was not performed. Template approach has some disadvantages. For instance, it is computationally demanding due to the great variation in sizes and shapes of microcalcifications. Another disadvantage is that it will fail if the pattern of the microcalcification is distorted or too noisy.

4.2. Microcalcification detection base on its features

A lot of research uses features extracted from mammogram to directly describe individual microcalcification. Nam and Choi [43] selected 7 features from a set of 29 features to evaluate seven classifiers. The features are: the area of the object, average grey level of the object, gradient strength of the object's perimeter pixels, root mean square (RMS) noise fluctuation, RMS noise fluctuation in an 3.5 mm × 3.5 mm local background, contrast (average grey level of the object minus the average grey level of a two pixel wide border surrounding the object), and a low order moment based on shape descriptor. With this set of features as the inputs, the linear classifier has the best performance. Veldkamp and Karssemeijer [81] also uses a large set of microcalcification features such as: perimeter, area, compactness, elongation, eccentricity, thickness, orientation, direction, line, the mean intensity level of the background, the mean intensity of the detected microcalcifications, and the contrast. These features form a feature vector, and their distributions are used as cluster features. With a KNN classifier, the method was tested on a set of 245 digitized mammograms having 341 clusters. The result showed that line/edge related features are more important at lower sensitivity. Zhang et al. [94] used a two-stage-scheme to reduce the false positive. Microcalcification features were divided into two categories: spatial features and morphology features. The first set of features includes: average gray level of the foreground, average gray-level of the background, standard deviation of the gray-level of the foreground, standard deviation of gray-level of the background. The second set of features includes: compactness, moment, and Fourier descriptor. Features to describe clusters are also used including spatial features, morphology features and the cluster description features. In the first stage, Zhang et al. [94] used a set of microcalcification features as the inputs of a back-propagation neural network to reduce the false detection. In the second stage, two more cluster features (cluster region size and cluster shape rate) are used as the inputs of the neural network to further reduce the false detection rate. Experimental results showed that the method could reduce the false detection rate by 42%, and a false detection rate of 3.15 per image was obtained. Davies et al. [95] used fewer features: area, mean gray level, ratio of area to the square of the maximum linear dimension, shape parameter, and edge strength. It can get 100% true positive rate and 5 false clusters on the 50 tested mammograms. We list several feature sets in Table 3.

4.3. Microcalcification detection based on statistical texture features

4.3.1. Surrounding region dependence method (SRDM)

This method is based on a second order histogram matrix which is calculated from two surrounding regions of a pixel [40,114]. Let us consider three rectangular windows centered at pixel (x, y), as shown in Fig. 4. R_1 and R_2 are the inner surrounding region and the outer surrounding region, respectively, and the values of ω_1, ω_2 and ω_3 denote the sizes of the three regions. A region of interest is transformed into a surrounding region-dependence matrix that is defined as

$$M(q) = [\alpha(i, j)], \quad 0 \leqslant i \leqslant m,\ 0 \leqslant j \leqslant n, \tag{15}$$

where q is a given threshold value and the values of m and n are the total numbers of the pixels in regions R_1 and R_2, respectively. In Eq. (15), the element $\alpha(i, j)$ is given as

$$\alpha(i, j) = \#\{(x, y) \,|\, C_{R_1}(x, y) = i$$

and

$$C_{R_2}(x, y) = j, (x, y) \in L_x \times L_y\}, \tag{16}$$

where # denotes the number of elements in the set, and $L_x \times L_y$ is the two-dimensional image space. In Eq. (16), the inner count $C_{R_1}(x, y)$ and the outer count $C_{R_2}(x, y)$ of the current pixel (x, y) are defined as follows:

$$C_{R_1}(x, y) = \#\{(k, l) \,|\, (k, l) \in R_1$$

and

$$[S(x, y) - S(k, l)] > q\}, \tag{17}$$

$$C_{R_2}(x, y) = \#\{(k, l) \,|\, (k, l) \in R$$

and

$$[S(x, y) - S(k, l)] > q\}, \tag{18}$$

where $S(x, y)$ is the image intensity of pixel (x, y). In general, the larger the thresholding value q is, the more microcalcifications could be missed, whereas the smaller the value q is, the more sensitive to the random noise and FP rate could be higher.

A set of four features can be extracted from the matrix:

(a) Horizontal-weighted sum (HWS)

$$HWS = \frac{1}{N} \sum_{i=0}^{m} \sum_{j=0}^{n} j^2 r(i, j). \tag{19}$$

Table 3
Features for microcalcification detection

Features	Details	References
Individual microcalcification features	Features extracted from mammogram directly such as perimeter, area, compactness, elongation, eccentricity, thickness, orientation, direction, line, background, foreground, distance, and contrast. They are easy to extract and they originate from the experience of radiologists.	[7,31,46,51,55,81,88,92,94–108]
Co-occurrence features	Features extracted from spatial gray level dependence matrix (co-occurrence matrix)	[7,100,109–113]
Surround region dependence (SRDM) features	Four directional-weighted sum extracted from the SRDM	[40,114]
Gray level run length (GLRL) features	Features extracted from the GLRL matrix	[40]
Gray level difference (GLD) features	Features extracted from the GLD matrix	[40,115]
Wavelet features	Energy, entropy, and norm extracted from the wavelet transform sub-images	[7,63,101,113,116–118]
Gabor filter bank features	Features extracted from gabor filter bank processed image	[108,119]
Scale-space features	Features extracted from the image processed by Laplacian of Gaussian filter	[86]
Fractal dimension	Features extracted from fractal model of the image	[109,117,119]
Cluster features	Features used to describe the distribution of the microcalcification, cluster area, and number of microcalcifications in an area	[3,51,81,88,94,95,100,120,121]

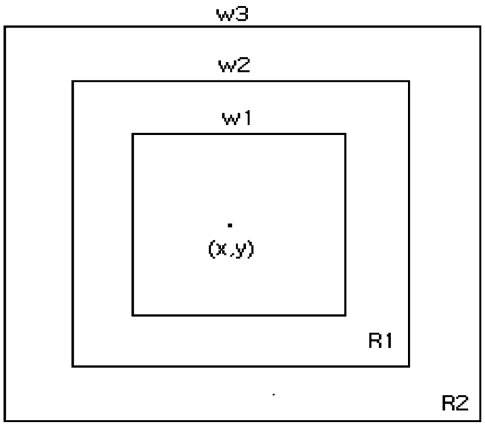

Fig. 4. Surrounding regions of pixel (x, y). R1 and R2 are the inner surrounding region and outer surrounding region, respectively. The values of $\omega1, \omega2$ and $\omega3$ denote the sizes of the three windows, respectively. [40].

(b) Vertical-weighted sum (VWS)

$$VWS = \frac{1}{N}\sum_{i=0}^{m}\sum_{j=0}^{n} i^2 r(i,j). \tag{20}$$

(c) Diagonal-weighted sum (DWS)

$$DWS = \frac{1}{N}\sum_{k=0}^{m+n} k^2 \left(\sum_{i=0}^{m}\sum_{j=0}^{n} r(i,j)\right), \quad i+j=k. \tag{21}$$

(d) Grid-weighted sum (GWS)

$$GWS = \frac{1}{N}\sum_{i=0}^{m}\sum_{j=0}^{n} ijr(i,j). \tag{22}$$

N is the number of total elements in the surrounding region dependence matrix,

$$N = \sum_{i=0}^{m}\sum_{j=0}^{n} \alpha(i,j) \tag{23}$$

and $r(i,j)$ is the reciprocal of the element, which is defined as:

$$r(i,j) = \begin{cases} 1/\alpha(i,j) & \text{if } \alpha(i,j) > 0, \\ 0 & \text{otherwise.} \end{cases} \tag{24}$$

4.3.2. Spatial gray level dependence method (SGLDM)

This method is based on an estimation of the second-order joint conditional probability density functions $P(i,j \mid d,\theta)$ for $\theta = 0°$, $45°$, $90°$, and $135°$. The function $P(i,j \mid d,\theta)$

is the probability that two pixels, that are located with an inter-sample distance d along direction θ, have gray level i and a gray level j, respectively. The estimated joint conditional probability density functions are defined as follows [40]:

$$p(i,j\mid d,0^\circ)=\#\{((k,l),(m,n))\in(L_x\times L_y)\times(L_x\times L_y)\mid l=n,|k-m|=d,S(k,l)=i,S(m,n)=j\}/T(d,0^\circ), \tag{25}$$

$$p(i,j\mid d,45^\circ)=\#\{((k,l),(m,n))\in(L_x\times L_y)\times(L_x\times L_y)\mid (k-m=-d,l-n=-d)\text{ or }(k-m=d,l-n=d),\ S(k,l)=i,S(m,n)=j\}/T(d,45^\circ), \tag{26}$$

$$p(i,j\mid d,90^\circ)=\#\{((k,l),(m,n))\in(L_x\times L_y)\times(L_x\times L_y)\mid (|l-n|=d,k=m,S(k,l)=i,S(m,n)=j\}/T(d,90^\circ), \tag{27}$$

$$p(i,j\mid d,135^\circ)=\#\{((k,l),(m,n))\in(L_x\times L_y)\times(L_x\times L_y):(k-m=-d,l-n=d)\text{ or }(k-m=d,l-n=-d),\ S(k,l)=i,S(m,n)=j\}/T(d,135^\circ), \tag{28}$$

where # denotes the number of elements in the set, $S(x,y)$ is the intensity of the pixel (x,y), and $T(d,\theta)$ stands for the total number of pixel pairs within the image which have the inter-sample distance d along direction θ.

Each of the estimated joint probability density functions can be written in a matrix form, and the spatial gray-level dependence matrix $\Phi(d,\theta)$ is as follows:

$$\Phi(d,\theta)=[p(i,j\mid d,\theta)],\quad 0\leqslant i,j\leqslant N_g, \tag{29}$$

where N_g is the maximum gray level. If the texture is coarse and d is small compared to the sizes of the texture elements, the pair of the pixels at the inter-sample distance d should usually have similar gray level. This means that the probability distribution in the matrix $\Phi(d,\theta)$ is concentrated on or near its diagonal. On the other hand, the gray levels of the points separated by the distance d should be quite different, therefore, the probability distribution in $\Phi(d,\theta)$ is away from its diagonal. The textural features can be extracted from the co-occurrence matrix. They are related to specific textural characteristics such as the homogeneity, contrast, entropy, energy and regularity of the structure within the image [100,109,110,112,113,122].

4.3.3. Gray level run length method (GLRLM)

This method is based on computing the number of gray level runs of various lengths [40]. A grey-level run is a set of consecutive and collinear pixel points having the same gray level value and its length is the number of pixel points in the run.

The gray level run length matrix is as follows:

$$R(\theta)=[g(i,j|\theta)],\quad 0\leqslant i\leqslant N_g,\quad 0\leqslant j\leqslant R_{\max}, \tag{30}$$

where N_g is the maximum gray-level and $R_{\max}$ is the maximum run length which is equal to $\max\{L_x,L_y\}$. The element $g(i,j|\theta)$ specifies the estimated number of times that a given image contains a run length j for a gray level i along direction θ. Four gray-level run-length matrixes along four different directions ($\theta=0^\circ$, 45°, 90°, and 135°) are computed for a ROI of size $L_x\times L_y$. Five features can be measured from the matrix $R(\theta)$: short run emphasis, long run emphasis, gray level nonuniformity, run length nonuniformity, and run percentage.

4.3.4. Gray level difference method (GLDM)

This method is based on the occurrence of two pixels that have a given absolute difference in gray levels and are separated by a specific displacement σ. For any given displacement vector $\sigma=(\Delta x,\Delta y)$, $S_\sigma(x,y)=|S(x,y)-S(x+\Delta x,y+\Delta y)|$ and $D(i\mid\sigma)$ is the estimated probability density function defined by

$$D(i\mid\sigma)=\Pr[S_\sigma(x,y)=i]. \tag{31}$$

Five features can be extracted from $D(i\mid\sigma)$: contrast, angular second moment, entropy, mean, and inverse difference moment [40,115].

Lee et al. [114] extracted four features from the SRD matrix of ROIs. A neural network could classify the regions as normal or microcalcification regions. Lee et al. [114] test the method on a set of 66 mammograms. The result shows that the detection sensitivity is 70.3% and specificity is 67.9%. Geronimo et al. [115] extract three features from co-occurrence matrix and two features from GLD matrix. Ferrari et al. [110] extracted a set of 13 SGLD features from 200 mammograms and using a multi-layer perceptron neural network, it got 88% correct rate to classify the microcalcification clusters as malignant or benign. Meersman et al. [112] extract raw features (the N^2-dimensional feature vector constructed by the normalized intensities of the pixels of a local $N\times N$ neighborhood centered at the candidate microcalcifications) and a set of 16 SGLD features from 40 mammograms of Nijmegen database and employes a multilayer feedforward neural network, it got 90% true positive microcalcification cluster detection rate with 1.2 false positive per image. Kim and Park [40] extracted features from SRD matrix, SGLD matrix, GLRL matrix, and GRD matrix, respectively. The test results on a set of 120 images show that the performance of SRD method, in terms of the area under the ROC curve, was superior to those of the other three methods in detecting microcalcification clusters.

4.4. Microcalcification detection based on multiscale texture features

4.4.1. Wavelet based method

Wavelet theory provides a powerful framework for multiresolution analysis, and it can be used for texture analysis [123,124]. The discrete wavelet transform is used to map the ROIs into a series of coefficients, which constituted a multiscale representation of the ROIs. To obtain the features reflecting scale-dependent properties, a set of features can be extracted from each scale of the wavelet transform. The most frequently used features are energy, entropy, and norm of the coefficients [7,63,101,113,117,118].

Yu et al. [101] used two wavelet transform coefficients and two local statistic features: median contrast and normalized gray level value. A 93% true positive and 1 false alarm per image was reported based on the tests of 40 images from Nijmegen database. Yu and Guan [7] further improved the performance by adding more features (a set of 31 features) extracted from microcalcification and co-occurrence matrix. It could reduce the false alarm rate to 0.5 per image. However the true positive detection rate is also dropped to 90%. Dhawan et al. [122] used texture features extracted from co-occurrence matrix and wavelets as the inputs to a radial-basis-function neural network. A maximum area 0.74 under ROC curve was obtained when using the method to detect the microcalcifications in 191 hard to diagnose mammograms. Dhawan et al. [113] increases this area to 0.86 by adding more cluster features. Zadeh et al. [118] extracted three kinds of features from ROIs: wavelet features, multi-wavelet features, and co-occurrence based features. Using a neural network, it could classify benign and malignant microcalcification clusters. The test results on a set of 103 regions containing microcalcifications show that the multi-wavelet method has better performance, and gets an area of 0.91 under the ROC curve.

4.4.2. Gabor filter bank method

Bhangale et al. [108] and Rogova et al. [119] used a set of Gabor filters to process mammograms. By changing the center frequencies of Gabor filters, this method could change the original images into different scales and orientation spaces. The filtered images are divided into small nonoverlapping blocks. For each block, the mean and standard deviation of the intensities are calculated and a feature vector is formed. Bhangale et al. [108] used a set of Gabor filters to process mammograms. By inputting the feature vectors extracted from the filtered image into a K-mean clustering classifier, it could get a 93.48% true positive and 1.09 false positive detection rate on 32 mammograms from Nijmegen database.

4.4.3. Laplacian of Gaussian method

Netsch and Peitgen [86] used a Laplacian of Gaussian filter to process mammograms. By changing the size of the filter, this method transforms the original image into different scale spaces. The Laplacian of Gaussian response at different scale is calculated as the features. By comparing Laplacian of Gaussian response of microcalcification with a predefined threshold, Netsch and Peitgen [86] could decide whether a spot is a microcalcification or not. The method was tested on the 40 mammograms of Nijmegen database and got 84% detect rate at the price of 1 false alarm per image.

4.5. Microcalcification detection based on fractal dimension features

Fractal dimension is a numerical value used to characterize a fractal, and it can be used as an indicator of the roughness of an image. Smoother areas of the images have lower fractal dimension values than rougher areas [109,119,125]. Caldwell et al. [125] used a simple method to calculate the fractal dimension of a mammogram. It supposed the mammogram was represented as 3D contours, and the third topological dimension was provided as a distance measure of each point's intensity. The calculation becomes a problem to measure the area of a 'mountainous' surface. The fractal dimension for the 'mountain' surface is related to the slope of a plot of $\log\{A(\varepsilon)\}$ versus $\log\{\varepsilon\}$. $A(\varepsilon) = \lambda\varepsilon^{2-D}$ is the area of the surface measured with a square of side ε, λ is a scaling constant, and D is a constant characteristic of the surface. By choosing two parameters, it could divide the microcalcifications into four Wolfe grades which are 'N1', 'P1', 'P2', and 'DY' [125]. It compared the classification result with those of four radiologists and 84% agreement has been got on a set of 70 mammograms. Enderwich and Tzanakou [109] calculated the fractal dimension from the slope of a log–log plot of ROIs. By combining features extracted from co-occurrence matrix, it achieved a 100% detection rate on a set of 24 microcalcification clusters using a neural network. Rogova et al. [119] calculated the fractal dimension of a mammogram based on alternating sequential filters. It extracted a four-dimension feature vector by using Gabor filter bank. These features were input into a neural network and 100% sensitivity and 41.6% specificity were achieved, comparing 89% sensitivity and 58.3% specificity obtained by radiologists when processing 40 mammograms from LLNL/UCSF database [119].

4.6. Microcalcification cluster detection using clustering features

After individual microcalcifications are detected, cluster features are used to group them into clusters. Zhang et al. [94] used spatial features, morphology features, and the cluster description features. Davies et al. [95,126] used the distance between the microcalcifications as a measure to group microcalcifications into clusters. Hojjatoleslami and Kittler [103] used the number of microcalcifications within a region of a fixed area. A square of 1 cm^2 is used as discontinuity measure to distinguish a new cluster. Nishlkawa et al. [121]

used the similar technology with [103]. However, it used 3 as the threshold while Hojjatoleslami and Kittler [103] used 4 as the threshold. There are some other features, nevertheless, cluster area and number of microcalcifications are the most popular cluster features due to their simplicity and effectiveness. The classifiers for MCCs detection are listed in Table 4.

5. Malignancy analysis

It is usually very difficult to distinguish benign from malignant MCCs because of the variability associated with their appearances. The human breast varies considerably in composition, and mammographic appearances varying from relative uniformity to complex patterns of bright streaks or blobs. The technologies similar to those in Section 6 are used for determining the malignancy. Here, we will discuss the feature sets, classifiers, and experimental results.

5.1. Feature sets

The feature sets are mainly the same with those used for microcalcification detection. They are: multiscale statistical features, wavelet features, co-occurrence features, surround region dependence features, individual microcalcification features, and cluster features. Table 5 lists the features used for malignant analysis.

5.2. Classifiers

Classifiers play an important role in the implementation of computer-aided diagnosis of mammography. The features or a subset of these features are employed by classifiers to classify microcalcifications into benign and malignant. A brief introduction of four kinds of classifiers is given here.

5.2.1. Neural networks

An artificial neural network is a parallel, distributed information processing structure consisting of processing elements interconnected by directional connections. A neural element carries out local operations. The key characteristics of the artificial neural networks is the distributed representation, local operations, and nonlinear processing. These attributes make artificial neural networks suitable for applications where only a few decisions are required from a massive amount of data, and also for the applications where a complex nonlinear relation needs to be learned. Thus, when the expert knowledge is not explicitly defined or cannot be represented in terms of statistically independent rules, artificial neural networks may provide a better solution than expert systems, and artificial neural networks can efficiently learn nonlinear mappings through examples contained in a training set, and conduct complex decision making. Finally, artificial neural networks can be effectively updated to learn new features. Dhawan et al. [111] used a backpropagation neural network by inputting a set of 10 SGLD features extracted from 85 difficult-to-diagnose mammograms, and obtained a classification accuracy of 74%. Verma and Zakos [8] also used a backpropagation neural network. A fuzzy technology is used to extract suspect regions and then features are extracted from the regions. The neural network could correctly classify 88.9% of the 40 cases from Nijmegen database. Jiang et al. [134] compared the classification result of neural network classifier with those of five radiologists. Experimental results showed that the neural network classifier had better performance than the radiologists in term of the area under the ROC curve (A_Z) and a partial area index ($_{0.90}A'_Z$). Patrocinio et al. [135] demonstrated that only several features such as irregularity, number of microcalcifications in a cluster, and cluster area, were needed as the inputs of a neural network to separate images into two distinct classes: suspicious and probably benign. An optimal neural network architecture selected by a simulated annealing optimization technique was used to improve the classification performance [136,137]. Genetic algorithms were also used to optimize features for differentiating malignant from benign [138–140].

5.2.2. K-nearest neighbor classifiers

K-nearest neighbor (KNN) classifier distinguishes unknown patterns based on the similarity to known samples. The KNN algorithm computes the distances from an unknown pattern to every sample and selects the K nearest samples as the base for classification. The unknown pattern is assigned to the class containing the most samples among the K-nearest samples.

Kramer and Aghdasi [129] used co-occurrence features and wavelet features as the inputs of a KNN classifier. 100% classification accuracy was achieved when classifying 40 images of Nijmegen database. Kramer and Aghdasi [127] compared the performances of KNN classifier and NN. The experiments showed that NN had better performance than KNN classifier. Zadeh et al. [133] used a set of shape features and co-occurrence features as the inputs of a KNN classifier. Using the 40 mammograms of Nijmegen database, it could only get an area of 0.82 under the ROC curves, which was much worse than that in Ref. [129]. Table 6 lists the classifiers and their performances.

5.2.3. Bayesian belief network (classifier)

Bayesian belief network (BBN) is an optimal pattern recognition method, which uses a probabilistic approach to determine an optimal segmentation given a specific database. A BBN builds an “acyclic” graph in which nodes represent feature variables, and connections between nodes represent direct probabilistic influences between the variables [145]. Each variable must have at least two discrete states and each state is associated with a probability value. For each node, the total of probability values for all states equal 1. If there is no path between any two nodes, it in-

Table 4
An overview of classifiers for MCCs detection

Classifiers	Results	References
Neural networks	88% correct rate in the test case of 200 images in USF database	[110]
	TP: 90% and FP: 1.2c/f, 40 images in Nijmegen database	[112]
	The area under ROC curve is 0.88, 120 images, source N/A	[40]
	TPF: 90% and FP: 0.77% on 30 images, source N/A	[46]
	93% mean TPF and FP 1c/f., 40 images in Nijmegen database	[101]
	90% mean TPF and FP 0.5c/f on 40 images in Nijmegen database	[7]
	100% sensitivity and 41.6% specificity the corresponding radiologists is 89% and 58.3% in 40 images in LLNL/UCSF	[119]
	TPF: 100% on MCC on 24MCC, source N/A	[109]
	TPF: 97.6% and FPF; 3.15c/f on 63 images in USUHS database	[94]
	TPF: 90% and FP; 1% 40 images in Nijmegen database	[96]
	Detection Rate: 88.89%. 5 images, source N/A	[97]
	90% TP, and less than half of the test images showing false images. 9 images: 288 samples with 144 for each class, source N/A	[98]
	TP 93% and FP: 1.5 c/f 27 images, source N/A	[99]
	TP: 90.6% on 128 ROIs, source N/A	[100]
	TP: 88.9%; 40 images in Nijmegen database	[8]
	Maximum area 0.86 under ROC, source N/A	[125]
	Area under ROC curve 0.935, 24 images, source N/A	[31]
K-nearest neighbor classifier	Maximum area 0.76 under ROC, 191 images, source N/A	[113]
	TPF: 100% and FP: 0.23 c/f , 80% correct rate and 0.25 c/f FP, 150 images from MIAS database	[103]
	TP: 80% and FP: 1 c/f , test image is generated by computer simulation	[3]
	Discussion is given on different parameter set, 245 images, source N/A	[81]
	TP: 85% and 0.1 FP, 40 images in Nijmegen database	[117]
	TP: 93.48 and FP: 1.09% on 32 images in Nijmegen database	[108]
	Area under ROC curve 0.929, 24 images, source N/A	[31]
	More than 80% classification accuracy on 180 images in Nijmegen LLNL/UCSF database	[127]
Bayesian classifier	TP: 92% with FP: 1c/f, 65 images, source N/A	[92]
	The agreement between this classifier and the radiologists is 84% on 70 images, source N/A	[125]
Quadratic classifier	Incorrect: 7.05%, Correct: 40%, Undecided: 52.86%, close to the mean performance of three expert radiologists 146 images, source N/A	[105,107]
	Area under ROC curve 0.918 on 24 images, source N/A	[31]
Linear classifier	TPF: 85% and FP: 1.5c/f, 78 images, source N/A	[106]
	Maximum area 0.70 under ROC, 70 images, source N/A	[125]
	Area under ROC curve 0.936, 24 images, source N/A	[31]
	TPF: 88% and FP: 1.1c/f, 50 image, source N/A	[128]
	TPF: 100% and FP: 5c/f, 50 images, source N/A	[51,95]
	TPF $>$ 85%, FP: 2c/f, 78 images, source N/A	[55,102]
	TPF: 85% and FP: 2.5c/f, 78 images, source N/A	[121]
Multiple expert system	The area under the ROC curve is 0.786, 40 images for USF	[120]
Fuzzy decision tree	Specificity: 73% and sensitivity: 60%, 118 images, source N/A	[88]
Binary decision tree	Area under ROC curve 0.9, 24 images, source N/A	[31]

c/f, clusters/frame. USF database: http://marathon.csee.usf.edu/Mammography/Database.html. Nijmegen database: http://marathon.csee.usf.edu/Mammography/OtherResources.html#NIJMEGEN. LLNL/UCSF database: http://marathon.csee.usf.edu/Mammography/OtherResources.html#LLNL. USUHS database: http://spaceline.usuhs.mil/. MIAS database: http://www.wiau.man.ac.uk/services/MIAS/MIASweb.html.

Table 5
Features for malignancy analysis

Features	Details	References
Multiscale statistical features	Features extracted from the spatial gray level dependence matrix which is calculated from the wavelet decomposition of the original mammogram	[127,129]
Wavelet features	Energy, entropy, and norm extracted from the wavelet transform sub-images	[122,130]
Co-occurrence features	Features extracted from the spatial gray level dependence matrix	[111,122,130–133]
Surround region dependence method (SRDM) features	Four directional-weighted sum extracted from SRDM	[114]
Individual microcalcification features	Features extracted from mammogram directly such as compactness, moments, average of the gray level, etc.	[8,33,131–135]
Cluster features	Features used to describe the distribution of the local features in the detected clusters: cluster area, and number of microcalcifications in an area.	[132–135]

Table 6
An overview of the classifiers for malignancy analysis

Classifier	Results	Studies
Neural networks	88.9% classification accuracy, 40 images in Nijmegen database	[8]
	A maximum area of 0.74 under ROC curve, 191 images source N/A	[122]
	An average of 0.6 under ROC curve, 191 'hard-to-diagnosis' images, source N/A	[132]
	88% accuracy, 94 'difficult to diagnose' cases, source N/A	[130]
	TPF $>$ 90%, 157 images, source N/A	[134]
	87% classification accuracy, 105 ROIs in LLNL	[141]
	Sensitivity: 79.5% and specificity: 85.1%, 285 images from Department of Radiology at Asian Medical Center, Seoul, Korea	[114]
	More than 90% classification accuracy, 180 images in Nijmegen and LLNL/UCSF database	[127]
K-nearest neighbor	The area under ROC curve is 0.82 for grey-level features, and 0.72 for SGLD features, 40 images in Nijmegen database	[133]
	Classification accuracy ranges form 71.08% to 83.13% with different settings, 180 images in Nijmegen and LLNL/UCSF database	[127]
	100% classification accuracy, 40 images in Nijmegen database	[129]
Bayesian classifier	Using 12 features, the area under the ROC for 433 images from Washington University Medical School in St. Louis was 0.873 ± 0.009	[142]
	The areas under ROC for linear and quadratic Bayesian classifier are 0.936 and 0.918 on a set of 24 mammograms, respectively. Source N/A	[31]
Decision tree	94% sensitivity can be achieved with 1.5 FP per image on a set of 50 normal and 45 abnormal mammograms. Database source N/A	[143]
	A sensitivity of 97.3% with 3.92 FP per image on 322 mammograms in the Mammographic Image Analysis Society Database.	[144]

dicates the probabilistic independence of two variables. In Refs. [99,146], a Bayesian classifier was used to merge five extracted features. The algorithm obtained a sensitivity of 100% with 0.22 false-clusters per mammogram on a test of 9 mammograms. In Ref. [31], seven classification methods, i.e., linear classifier, quadratic classifier, binary decision trees, backpropagation neural network, the cascade correlation neural network, the divide and conquer neural network and k-nearest neighbors algorithm, are compared on a set of 24 mammograms, each of them contains at least one biopsy-proven malignant cluster of microcalcifications. The result showed that Bayesian classifiers outperformed three types of artificial neural networks. The Bayesian techniques and artificial neural network are able to produce many ROC points, which indicate there are inherent flexibilities of these classifiers. In Refs. [142,147], common databases and the same genetic algorithm were used to optimize both Bayesian belief network and neural network. The results

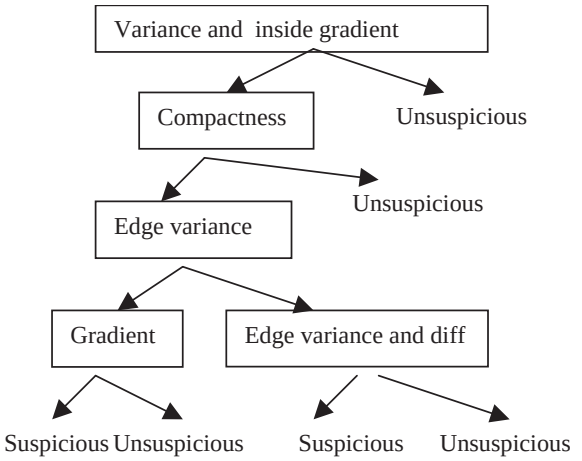

Fig. 5. The structure of a binary decision tree [144].

showed that the performance of the two techniques converged to the same level, therefore, it was concluded that the performance of CAD system might be more dependent on feature selection and training database than on any particular classifier [142,147]. Bayesian methods have also been applied to artificial neural networks in order to regularize training to improve the robustness of the classifier [148,149].

5.2.4. Binary decision tree

Binary decision tree is an ordered list of binary threshold operations on the features organized as a tree. Each node will move down to its two descendents by thresholding values of the features. This procedure will continue until it arrives at a terminal node which assigns a classification. The control parameters at each node are selected by simply determining the feature and threshold that best separates the current data into two classes. The process recursively partitions the remaining training samples and generates a tree. Comparing with neural networks, the decision tree approach is much simpler with low computational overhead. And it also does not need extensive knowledge of the probability distribution of the features like Bayesian classifier.

Fig. 5 shows an example of decision tree [144].

Fuzzy logic can improve the performance of decision tree [88,143,150,151]. Fuzzy subset allows taking into account a grading of membership which is useful to follow a different path for two values located on both sides of the threshold of the test. In Ref. [88], fuzzy decision tree was used as the classifier of the 82 images, and a specificity of 92% with a sensitivity of 96% was obtained. Comparing the performance of fuzzy decision tree with several different approaches (KNN, Bayesian ID3), the fuzzy decision tree outperformed others [88].

6. Evaluation for detection algorithms

6.1. Sensitivity and specificity

Usually, an image region can be called cancerous (positive) or normal (negative), and a decision for a detection result can be either correct (true) or incorrect (false). A decision for a detection result, therefore, will be one of four possible categories as shown in Table 7 [152]: true positive (TP), true negative (TN), false positive (FP), and false negative (FN). FN and FP are two kinds of errors. A false negative error implies that a true abnormality was not detected, and a false positive error occurs when a normal region was falsely identified as abnormality. A TP decision is a correct judgment of an actual abnormality, and a TN decision means a normal region was correctly labeled.

For years, the performance of diagnostic systems has been measured and reported in terms of a kind of "percent correct" which is the percentage of diagnostic decisions that proved to be correct [153]. But the "percent correct" measure depends strongly on disease prevalence and cannot reveal the relative rates of false positive and false negative errors. These disadvantages can be overcome by using a pair of indices: "sensitivity" and "specificity". The terms "sensitivity" and "specificity" are synonymous with true positive and true negative rate (or ratio, or fraction), respectively. That is $sensitivity = TPs/(TPs + FNs)$ and $specificity = TNs/(TNs + FPs)$.

However, if one just uses the sensitivity and specificity parameters to compare the performance of two systems, there has a dilemma in which one system provides higher sensitivity, meanwhile lower specificity than the other [154]. For a fixed discrimination capacity, the sensitivity and specificity of a diagnostic system will depend on the particular confidence threshold that the observer or the computer diagnostic system uses to partition continuously distributed perceptions of evidence into categorical decisions. Both sensitivity and specificity will change if the confidence threshold is changed [153]. A solution to this problem is suggested by the use of ROC (receiver operating characteristic) curve which indicates the tradeoffs between sensitivity and specificity that are available from a diagnostic system, and thus describes the inherent discrimination capacity of that system.

Table 7
A decision made on a detection task [152]

	True state	
CAD	A cancer	Not a cancer
Claimed A cancer	True Positive	False Positive
Not claimed A cancer	False Negative	True Negative

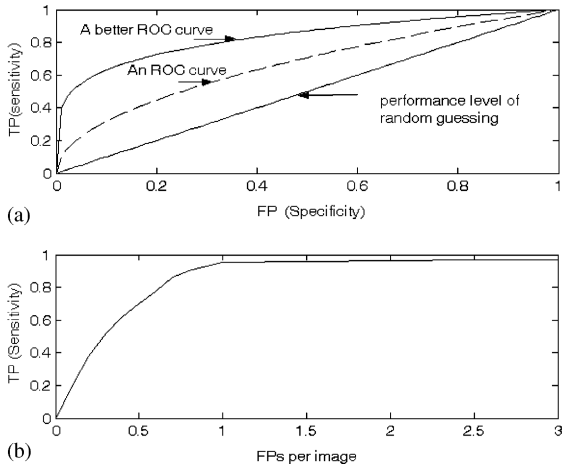

Fig. 6. (a) ROC curves and (b) FROC curve [152].

6.2. ROC and FROC curve analysis

Receiver operating characteristic (ROC) analysis is a well known evaluation method for detection tasks [153–158]. It is based on statistical decision theory and first developed in signal detection theory [159]. In [160–162], ROC analysis was first used in medical decision making. Subsequently, it was used in medical imaging. An ROC curve is a plot of operating points which can be considered as a plotting of true positive as a function of false positive. When we design a computer-aided diagnosis system, generating operating points is usually done by applying thresholds to the detection algorithm outputs that roughly correspond to the concept of confidence thresholds used by human observers. Most statistical classifiers produce outputs that can be easily thresholded to generate a large number of operating points. A typical ROC curve is shown in Fig. 6(a) [152]. A higher ROC, approaching the perfection at the upper left hand corner, would indicate greater discrimination capacity. The CLABROC program is a kind of procedures employed to test the statistical significance of the difference between two ROC curves [163]. In this program, a bivariate chi-square test is applied to the difference between the a parameters (y-intercepts on the normal-deviate axes) and the b parameters (the slopes of straight lines on the normal deviate axes) of the two ROC curves.

For evaluating true-positive detection, sometimes it is required not only the existence but also the localization of the tumor. A better method for this case is free-response receiver operating characteristic (FROC) analysis which is a plot of operating points showing the tradeoff between the TP rate versus the average number of false positives per image [152,164–166]. A FROC curve is shown in Fig. 6(b). The difference between FROC and ROC methods can be displayed by the abscissa of the FROC plot that begins at zero and no upper limit, while the abscissa of the ROC plot is from zero to one. The ordinate of an FROC curve is 0–100% sensitivity, the same as for ROC curve. However, both FROC and ROC analysis suffer from their limitations. For instance, they do not address the complexity of images and are difficult to transform the subjective measurements (radiologist's observations) to the objective FROC curve.

6.3. A_Z values computing

The area under the ROC curve or the FROC curve is an important criterion for evaluating diagnostic performance [153,154]. Usually it is referred as the A_Z index. The A_Z value of ROC curve is just the area under the ROC curve. The A_Z value of FROC curve should be computed by normalizing the area under the FROC curve by the range of the abscissa. The value of A_Z is 1.0 when the diagnostic detection has perfect performance which means that TP rate is 100% and FP rate is 0%. The ROCFIT program [167] is for estimating A_Z from the observer responses in the ROC experiment. The method assumes that the observers make a yes/no decision on each image, depending on whether the decision variable exceeds a threshold value. The estimation of the A_Z value can be obtained with the trapezoidal rule which can underestimate areas under the curve. More operating points are generated, less underestimation error will be obtained. The A_Z value can also be computed by fitting a continuous binormal curve to the operating points, provided the functional form of the ROC curve is given [153].

7. Conclusions

Automated breast cancer detection has been studied for more than 20 years, the CAD mammography systems for microcalcification detection have gone from crude tools in the research laboratory to commercial systems. Several commercial companies such as R2 Technology Inc., Hewlett Packard Co., Sterling Diagnostic Imaging, Siemens, GE, MedDetect/Lockheed Martin, were developing or designing mammography systems for clinical applications. R2 Technology Inc. has produced a system ImageChecker® for MCCs and mass detection. It received the approval from the US Food and Drug Administration (FDA) in June 1998 and from the Japanese Ministry of Health and Welfare (MHW) for use of the ImageChecker System in breast cancer screening in February 2000. It also received CE Mark certification from the European Union. The performance obtained on a large, consecutive set of cancer cases can be as high as 98.3% sensitivity with a false-positive rate of 0.3 clusters per image [168,169].

Although by now some progress has been achieved, there are still remaining challenges and directions for future research, such as

- Developing better enhancement and segmentation algorithms.

- Designing better feature detection and selection algorithms.
- Integration of classifiers to reduce both FPs and FNs. In order to reduce false positive, several different types of features, sometimes, with clinical information should be used. As the complexity of algorithm increases, the time complexity of the CAD will also increase. How to keep the balance between the accuracy and computational complexity is quite important since long time delay could make the clinical use of a CAD system less attractive [170,171].
- Defining a standard test set (database) and better evaluation criteria are still very important. With some rigorous evaluations, and objective and fair comparison could determine the relative merit of competing algorithms and facilitate the development of better and robust systems [16,152].
- Employing high resolution mammograms. Although it was suggested that a pixel matrix of at least 2048×2560 be the minimum spatial resolution required for digital mammography [25,172], the spatial resolution and dynamic range (gray-levels per pixel) required to adequately representing microcalcifications in a digitized film mammogram is still an open question. It requires high resolution to see fine details and wide dynamic range to capture in a single image structures, and low light sensitivity to shorten exposure and reduce X-ray dosage.
- Integrating other imaging modalities with X-ray mammography. Although CAD for mammography uses mainly X-ray mammography, there are some alternatives [173–176]. Ultrasound has been used as an adjunct to mammography in detecting breast cancer [175]. Although the result of sensitivity is still low comparing with mammograph, [177] showed a result with a sensitivity of 95% and specificity of 87% in the detection of microcalcifications that indicated the perspective for future improvement. Grable et al. [174] described vibro-acoustography based on radiation force of ultrasound. The spatial resolution of vibro-acoustography is in the submillimeter range which makes the technique suitable for imaging microcalcification [178]. The ultrasound energy can easily penetrate dense tissues which are opaque and difficult to X-ray. The method can be a nonionizing alternative to conventional X-ray mammography to detect microcalcifications in women of pregnant, lactating, with radio-opaque breast implants, or with dense tissue. Further development of ultrasound, MRI and CT combined with X-ray mammography may lead to a novel effective CAD system for breast cancer control.
- Investigating 3D mammograms. Mammograms are two-dimension representations of three-dimensional structures. The spatial distribution of the microcalcification clusters is inevitably distorted in the projected two-dimension mammograms and will loss the depth and location of the imaged structures. Although the research on the three-dimension mammograms is much less than that on the brain, heart, or lung [179–182], recently three-dimension visualization and analysis of breast has aroused growing interest. Some new mammographic technologies generating and combining multiple views of the breast, and 3-D mammogram reconstruction have been studied [183–185]. Enhancement and segmentation methods have been studied for three-dimension images [182,186]. To develop new and better imaging processing algorithms for three-dimension mammograms is still a big challenge.

References

[1] X. Zhou, R. Gordon, Detection of early breast cancer: an overview and future prospects, Crit. Rev. Biomed. Eng. 17 (1989) 203–255.

[2] H.P. Chan, K. Doi, C.J. Vyborny, K.L. Lam, R.A. Schmidt, Computer-aided detection of microcalcifications in mammograms—methodology and preliminary clinical study, Invest. Radiol. 23 (9) (1988) 664–671.

[3] H.P. Chan, K. Doi, S. Galhotra, C.J. Vyborny, H. MacMahon, P.M. Jokich, Image feature analysis and computer-aided diagnosis in digital radiography I. Automated detection of microcalcifications in mammography, Med. Phys. 14 (4) (1987) 538–548.

[4] Y. Wu, K. Doi, M.L. Giger, R.M. Nishikawa, Computer-aided detection of microcalcifications in digital mammograms, Invest. Radiol. 9 (1988) 664–674.

[5] D.H. Davies, D.R. Dance, The automatic computer detection of subtle calcifications in radiographically dense breasts, Phys. Med. Biol. 37 (1992) 1385–1390.

[6] S. Lee, C. Lo, C. Wang, P. Chung, C. Chang, C. Yang, P. Hsu, A computer-aided design mammography screening system for detection and classification of microcalcifications, Int. J. Med. Inform. 60 (1) (2000) 29–57.

[7] S. Yu, L. Guan, A CAD system for the automatic detection of clustered microcalcifications in digitized mammogram films, IEEE Trans. Med. Imag. 19 (2) (2000) 115–126.

[8] B. Verma, J. Zakos, A computer-aided diagnosis system for digital mammograms based on fuzzy-neural and feature extraction techniques, IEEE Trans. Inform. Technol. Biomed. 5 (1) (2001) 46–54.

[9] H. Yoshida, K. Doi, R.M. Nishikawa, M.L. Giger, R.A. Schmidt, An improved computer-assisted diagnostic scheme using wavelet transform for detecting clustered microcalcifications in digital mammograms, Acad. Radiol. 3 (8) (1996) 621–627.

[10] B. Zheng, Y. Chang, M. Staiger, W. Good, D. Gur, Computer-aided detection of clustered microcalcifications in digitized mammograms, Acad. Radiol. 2 (1995) 655–662.

[11] M. Wilson, S. Mitra, G.H. Roberson, Y.Y. Shieh, Automated microcalcification detection in mammograms using statistical-variable box-threshold filter method, SPIE 3165 (1997) 195–326.

[12] M.A. Gavrielides, J.Y. Lo, Jr CE, Parameter optimization of a computer-aided diagnosis scheme for the segmentation of microcalcification clusters in mammograms, Med. Phys. 29(4) (2002) 475–483.

[13] A. Papadopoulos, D.I. Fotiadis, A. Likas, An automatic microcalcification detection system based on a hybrid neural network classifier, Artif. Intell. Med. 25 (2) (2002) 149–167.
[14] B. Verma, J. Zakos, A computer-aided diagnosis system for digital mammograms based on fuzzy-neural and feature extraction techniques, IEEE Trans. Inform. Technol. Biomed. 5 (1) (2001) 46–54.
[15] I. Leichter, R. Lederman, S. Buchbinder, P. Bamberger, B. Novak, S. Fields, Optimizing parameters for computer-aided diagnosis of microcalcifications at mammography, Acad. Radiol. 7 (6) (2000) 406–412.
[16] R.M. Nishikawa, Detection of microcalcification, in: N. Karssemeijer, M. Thijssen, J. Hendriks, L. van Erning (Eds.), Digital Mammography Nijmegen 98, Kluwer Academic Publisher, Amsterdam, 1998, pp. 131–153.
[17] S.L. Olson, B.W. Fam, P.F. Winter, F.J. Scholz, A.K. Lee, S.E. Gordon, Breast calcifications: analysis of imaging properties, Radiology 169 (2) (1988) 329–332.
[18] A.P. Dhawan, E.L. Royer, Mammographic feature enhancement by computerized image processing, Comput. Methods Programs Biomed. 27 (1) (1988) 23–35.
[19] E.A. Sickles, Mammographic features of 300 consecutive nonpalpable breast cancers, Am. J. Radiol. 146 (1986) 661–665.
[20] A. Beghdadi, A.L. Negrate, Contrast enhancement technique based on local detection of edges, Comput. Vision Graphics Image Process. 46 (1989) 162–174.
[21] J. Dengler, S. Behrens, J.F. Desaga, Segmentation of microcalcifications in mammograms, IEEE Trans. Med. Imag. 12 (4) (1993) 634–642.
[22] H.D. Cheng, H.J. Xu, Fuzzy approach to contrast enhancement, 14th International Conference on Pattern Recognition, Brisbane, Australia, August 1998, pp. 17–22.
[23] N. Karssemeijer, Adaptive noise equalization and image analysis in mammography, Information Processing in Medical Imaging: 13th International Conference, IPMI '93, AZ, USA, 1993, pp. 472–486.
[24] M.B. McSweeney, P. Sprawls, R.L. Egan, Enhanced image mammography, AJR 140 (1983) 9–14.
[25] H.P. Chan, C.J. Vyborny, H. McaMahon, C.E. Metz, K. Doi, E.A. Sickles, Digital mammography: ROC studies of the effects of pixel size and unsharp-mask filtering on the detection of subtle microcalcifications, Invest. Radiol. 22 (7) (1987) 581–589.
[26] K. Woods, L.P. Clarke, R. Velthuizen, Enhancement of digital mammograms using a local thresholding technique, Annual International Conference of the IEEE Engineering in Medicine and Biology Society 13 (1) (1991) 114–115.
[27] R. Gordon, R.M. Rangayyan, Feature enhancement of film mammograms using fixed and adaptive neighborhoods, Appl. Opt. 23 (4) (1984) 560–564.
[28] A.P. Dhawan, G. Buelloni, R. Gordon, Enhancement of mammographic features by optimal adaptive neighborhood image processing, IEEE Trans. Med. Imag. MI-5 (1) (1986) 8–15.
[29] W.M. Morrow, R.B. Paranjape, R.M. Rangayyan, J.E.L. Desautels, Region-based contrast enhancement of mammograms, IEEE Trans. Med. Imag. 11 (3) (1992) 392–406.
[30] M. Kallergi, K. Woods, L.P. Clarke, W. Qian, R.A. Clark, Image segmentation in digital mammography: comparison of local thresholding and region growing algorithms, Comput. Med. Imag. Graph. 16 (1992) 323–331.
[31] K.S. Woods, C.C. Doss, K.W. Bowyer, J.L. Solka, C.E. Priebe, W.P. Kegelmeyer, Comparative evaluation of pattern recognition techniques for detection of microcalcifications in mammography, Int. J. Pattern Recognition Artif. Intell. 7 (1993) 1417–1436.
[32] L. Shen, R. Rangayyan, J.E.L. Desautles, Detection and classification of mammographic calcifications, Int. J. Pattern Recognition Artif. Intell. 7 (1993) 1403–1416.
[33] L. Shen, R.M. Rangayyan, J.E.L. Desautels, Application of shape analysis to mammographic calcifications, IEEE Trans. Med. Imag. 13 (2) (1994) 263–274.
[34] M.N. Gurcan, Y. Yardimci, A.E. Cetin, R. Ansari, Detection of microcalcifications in mammograms using higher order statistics, Signal Process. Lett. 4 (8) (1997) 213–216.
[35] M.N. Gurcan, Y. Yardimci, A.E. Cetin, R. Ansari, Automated detection and enhancement of microcalcifications in mammograms using nonlinear subband decomposition, 1997 IEEE International Conference on Acoustics, Speech, and Signal Processing, Vol. 4, Munich, Germany, April 1997, pp. 3069–2072.
[36] H.D. Cheng, Y.M. Lui, R.I. Freimanis, A novel approach to microcalcification detection using fuzzy logic technique, IEEE Trans. Med. Imag. 17 (3) (1998) 442–450.
[37] A.F. Laine, S. Schuler, J. Fan, W. Huda, Mammographic feature enhancement by multiscale analysis, IEEE Trans. Med. Imag. 13 (4) (1994) 7250–7260.
[38] J.K. Kim, J.M. Park, K.S. Song, H.W. Park, Adaptive mammographic image enhancement using first derivative and local statistics, IEEE Trans. Med. Imaging. 16 (5) (1997) 495–502.
[39] J.K. Kim, J.M. Park, S.S. Song, H.W. Park, Detection of clustered microcalcifications on mammograms using surrounding region dependence method and artificial neural network, J. VLSI Signal Process. 18 (1998) 251–262.
[40] J.K. Kim, H.W. Park, Statistical textural features for detection of microcalcifications in digitized mammograms, IEEE Trans. Med. Imag. 18 (3) (1999) 231–238.
[41] H. Li, K.J. Ray Liu, S.C.B. Lo, Fractal modeling and segmentation for the enhancement of microcalcifications in digital mammograms, IEEE Trans. Med. Imag. 16 (6) (1997) 785–798.
[42] H. Li, K.J.R. Liu, S.C.B. Lo, Fractal modeling of mammogram and enhancement of microcalcifications, 1996 IEEE Nuclear Science Symposium & Medical Imaging Conference, Vol. 3, 1996, pp. 1850–1854.
[43] S.H. Nam, J.Y. Choi, A methods of image enhancement and fractal dimension for detection of microcalcifications in mammogram, Proceedings of the 20th Annual International Conference of the IEEE Engineering in Medicine and Biology Society, Vol. 20 (2), 1998, pp. 1009–1012.
[44] S. Yu, S. Brown, Y. Xue, L. Guan, Enhancement and identification of microcalcifications in mammogram images using wavelets, 1996 IEEE International Conference on Systems, Man and Cybernetics, Vol. 2, Beijing China, October 1996, pp. 1166–1171.
[45] T.C. Wang, N.B. Karayiannis, Detection of microcalcifications in digital mammograms using wavelets, IEEE Trans. Med. Imag. 17 (4) (1998) 498–509.
[46] B. Zheng, W. Qian, L.P. Clarke, Digital mammography: mixed feature neural network with spectral entropy decision

for detection of microcalcifications, IEEE Trans. Med. Imag. 15 (5) (1996) 589–597.
[47] H. Yoshida, K. Doi, R.M. Nishikawa, Automated detection of clustered microcalcifications, SPIE Image Processing, Vol. 2167, Newport Beach, CA, February 1994, pp. 868–886.
[48] L.N. Mascio, J.M. Hernandez, C.M. Logan, Automated analysis for microcalcifications in high resolution digital mammograms, SPIE Image Process. 1898 (1993) 472–479.
[49] H. Cheng, Y. Lui, R. Freimanis, A novel approach to microcalcification detection using fuzzy logic technique, IEEE Trans. Med. Imag. 17 (3) (1998).
[50] F. Lefebvre, H. Benali, E. Kahn, R.D. Paola, A fractal approach to the segmentation of microcalcifications in digital mammograms, Med. Phys. 22 (4) (1995) 381–391.
[51] D.H. Davies, D.R. Dance, Automatic computer detection of clustered calcifications in digital mammograms, Phys. Med. Biol. 35 (1990) 1111–1118.
[52] I.N. Bankman, T. Nizialek, I. Simon, O.B. Gatewood, I.N. Weinberg, W.R. Brody, Segmentation algorithms for detecting microcalcifications in mammograms, IEEE Trans. Med. Imag. 1 (2) (1997) 141–149.
[53] M. Kass, A. Witken, D. Terzopoulos, Snakes: active contour models, Int. J. Comput. Vision 1 (4) (1988) 321–331.
[54] J.M. Mossi, A. Albiol, Improving detection of clustered microcalcifications using morphological connected operators, 1999 IEEE Image Processing and its Applications, 1999, pp. 498–501.
[55] R.M. Nishikawa, Y. Jiang, M.L. Giger, K. Doi, C.J. Vyborny, R.A. Schmidt, Computer-aided detection of clustered microcalcifications, Proceedings of the IEEE International Conference on Systems, Man and Cybernetics, 1992, pp. 1375–1378.
[56] D. Zhao, M. Shridhar, D.G. Daul, Morphology on detection of calcifications in mammograms, 1992 IEEE International Conference on Acoustics, Speech and Signal Processing, III, March 23–26, 1992, pp. 129–132.
[57] H.R. Jin, Extraction of microcalcifications from mammograms using morphological filter with multiple structuring elements, System Comput. Jpn. 24 (11) (1993) 66–74.
[58] C.H. Chen, G.G. Lee, On digital mammogram segmentation and microcalcification detection using multiresolution wavelet analysis, Graphical Models Image Process. 59 (5) (1997) 349–364.
[59] J.J. Heine, S.R. Deans, D.K. Cullers, R. Stauduhar, L.P. Clarke, Multiresolution statistical analysis of high-resolution digital mammograms, IEEE Trans. Med. Imag. 16 (5) (1997) 503–515.
[60] H. Yoshida, W. Zhang, W. Cai, K. Doi, R.M. Nishikawa, M.L. Giger, Optimizing wavelet transform based on supervised learning for detection of microcalcifications in digital mammograms, Proceedings of the IEEE International Conference on Image Processing, Vol. 3, Washington, DC, October 1995, pp. 152–155.
[61] R.N. Strickland, H.I. Hahn, Wavelet transforms for detecting microcalcifications in mammography, Proceedings of the International Conference on Image Processing, Austin, TX, 1994, pp. 402–406.
[62] R.N. Strickland, H.I. Hahn, Wavelet transform matched filters for the detection and classification of microcalcifications in mammography, Proceedings of the 1995 IEEE International Conference on Image Processing, October 23–28, 1995, pp. 422–425.
[63] R.N. Strickland, H.I. Hahn, L.J. Baig, Wavelet methods for combining CAD with enhancement of mammograms, Medical Imaging 1996: Image Processing, SPIE Proceedings, Vol. 2710, 1996, pp. 888–903.
[64] R.N. Strickland, H.I. Hahn, Wavelet transform methods for object detection and recovery, IEEE Trans. Image Process. 6 (1997) 724–735.
[65] W.J.H. Veldkamp, N. Karssemeijer, Normalization of local contrast in mammograms, IEEE Trans. Med. Imag. 19 (7) July, (2000) 731–738.
[66] B.J. Lucier, M. Kallergi, W. Qian, R.A. DeVore, R.A. Clark, E.B. Saff, L.P. Clarke, Wavelet compression and segmentation of digital mammograms, J. Digital Imag. 7 (1) (1994) 27–38.
[67] X.P. Zhang, M.D. Desai, Segmentation of bright targets using wavelets and adaptive thresholding, IEEE Trans. Image Process. 10 (7) (2001) 1020–1030.
[68] L.P. Clarke, M. Kallergi, W. Qian, H.D. Li, R.A. Clark, M.L. Silbiger, Tree-structured non-linear filter and wavelet transform for microcalcification segmentation in digital mammography, Cancer Lett. 77 (1994) 173–181.
[69] W. Qian, M. Kallergi, L.P. Clarke, H.D. Li, P. Venugopal, Tree structured wavelet transform segmentation of microcalcifications in digital mammography, Med. Phys. 22 (8) (1995) 1247–1253.
[70] R.N. Strickland, H. II Hahn, The wavelet transform as a multiresolution matched filter and zero-crossing detector for detecting microcalcifications in mammograms, Proceedings of the 1995 IEEE Engineering in Medicine and Biology 17th Annual Conference and 21st Canadian Medical and Biological Engineering Conference, September 20–23, 1995, pp. 1047–1048.
[71] L. Donald, A. McCandless, S.K. Rogers, M.J.W. Hoffmeigter, M.D.W. Ruck, C.R.A. Raines, B.W. Suter, Wavelet detection of clustered microcalcifications, Proc. SPIE—Int. Soc. Opt. Eng. 2762 (1996) 388–399.
[72] D. Gunawan, Microcalcification detection using wavelet transform, IEEE Pacific RIM Conference on Communications, Computers and Signal Processing, August 26–28, 2001, pp. 694–697.
[73] H.C. Choe, A.K. Chan, Microcalcification cluster detection in digitized mammograms using multiscale techniques, Proceedings of the IEEE Southwest Symposium on Image Analysis and Interpretation, 1998, pp. 23–28.
[74] W. Qian, L.P. Clarke, H.D. Li, R.A. Clark, M.L. Silbiger, Adaptive order statistic filtering and wavelet transform for feature enhancement in mammography, Proceedings of the Annual Conference on Engineering in Medicine and Biology, Vol. 15 (part 1), October 28–31, 1993, pp. 62–63.
[75] M.J. Lado, P.G. Tahoces, A.J. Mendez, M. Souto, J.J. Vidal, A wavelet-based algorithm for detecting clustered microcalcifications in digital mammograms, Med. Phys. 26 (7) (1999) 1294–1305.
[76] W. Qian, L.P. Clarke, M. Kallergi, R.A. Clark, Tree-structured nonlinear filters in digital mammography, IEEE Trans. Med. Imag. 13 (1) (1994) 25–36.
[77] T.W. Cheng, D.B. Goldgof, L. Hall, Fast fuzzy clustering, Fuzzy Sets and Systems 93 (1998) 49–56.
[78] N. Karssemeijer, Adaptive noise equalization and recognition of microcalcification clusters in mammograms, Int. J. Pattern Recognition Artif. Intell. 7 (6) (1993) 1357–1376.

[79] R.N. Strickland, H.II. Hahn, Wavelet transforms for detecting microcalcifications in mammograms, IEEE Trans. Med. Imag. 15 (2) (1996) 218–229.

[80] B.W. Fam, S.L. Olson, P.F. Winter, F.J. Scholz, Algorithm for the detection of fine clustered calcifications on film mammograms, Radiology 169 (2) (1988) 333–337.

[81] W.J.H. Veldkamp, N. Karssemeijer, An improved method for detection of microcalcification clusters in digital mammograms, The SPIE Conference on Image Processing, Vol. 3661, February 1999, pp. 512–522.

[82] N. Karssemeijer, A stochastic model for automated detection of calcifications in digital mammograms, 12th International Conference IPMI, Wye, UK, 1992, pp. 227–238.

[83] B.C. Wallet, J.L. Solka, C.E. Priebe, A method for detecting microcalcifications in digital mammograms, J. Digital Imag. 10 (3) (1997) 136–139.

[84] D. Song, W. Qian, L.P. Clarke, Digital mammography: hybrid M-channel wavelet transform for microcalcification segmentation, 18th Annual International Conference of the IEEE Engineering in Medicine and Biology Society, Amsterdam, 1996, pp. 1069–1070.

[85] S. Dippel, M. Stahl, R. Wiemker, T. Blaffert, Multiscale contrast enhancement for radiographies: Laplacian pyramid versus fast wavelet transform, IEEE Trans. Med. Imag. 21 (4) (2002) 343–353.

[86] T. Netsch, H.O. Peitgen, Scale-space signatures for the detection of clustered microcalcifications in digital mammograms, IEEE Trans. Med. Imag. 18 (9) (1999) 774–786.

[87] T. Netsch, A scale-space approach for the detection of clustered microcalcifications in digital mammograms, Digital Mammography'96, Proceedings of the Third International Workshop Digital Mammography, Chicago, IL, June 1996, pp. 301–306.

[88] S. Bothorel, B.B. Meunier, S. Muller, A fuzzy logic based approach for semiological analysis of microcalcifications in mammographic images, Int. J. Intelligent Systems 12 (1997) 819–848.

[89] H.D. Cheng, J.R. Chen, R.I. Freimanis, X.H. Jiang, A novel fuzzy logic approach to microcalcification detection, J. Inform. Sci. (1998) 1–14.

[90] N. Pandey, Z. Salcic, J. Sivaswamy, Fuzzy logic based microcalcification detection, Neural Networks for Signal Processing—Proceedings of the IEEE Workshop, Vol. 2, December 11–13, 2000, pp. 662–671.

[91] J.C. Olivo, Automatic detection of spots in biological images by a wavelet-based selective filtering technique, Proceedings of the 1996 IEEE International Conference on Image Processing, September 16–19, 1996, pp. 311–314.

[92] N. Karssemeijer, Recognition of microcalcification clusters in mammograms, Int. J. Pattern Recognition Artif. Intell. 7 (6) (1993) 1357–1376.

[93] S. Morrison, L.M. Linnett, A model based approach to object detection in digital mammography, IEEE Int. Conf. Image Process. 2 (1999) 182–186.

[94] L. Zhang, W. Qian, R. Sankar, D. Song, R. Clark, A new false positive reduction method for MCCs detection in digital mammography, IEEE International Conference on Acoustics, Speech and Signal Processing, May 7–11, 2001, pp. 1033–1036.

[95] D.H. Davies, D.R. Dance, C.H. Jones, Automatic detection of clusters of calcifications in digital mammograms, SPIE Med. Imag. IV: Image Process. 1233 (1990) 185–191.

[96] C.H. Chen, G.G. Lee, Image segmentation using multi-resolution wavelet analysis and expectation-maximization (EM) algorithm for digital mammography, J. Digital Imag. 8 (1997) 491–504.

[97] S. Sehad, S. Desarnaud, A. Strauss, Artificial neural classification of clustered microcalcifications on digitized mammograms, Proceedings of the IEEE International Conference on Systems, Man and Cybernetics, Vol. 5, 1997, pp. 4217–4222.

[98] K. Woods, C. Doss, K. Bowyer, L. Clarke, R. Clark, A neural network approach to microcalcification detection, IEEE 1992 Nuclear Science Symposium and Medical Imaging Conference, Orlando, FL (October 1992), 1992, pp. 1273–1275.

[99] Bankman, J. Tsai, D. Kim, O. Gatewood, W. Brody, Detection of microcalcification clusters using neural networks, Annual International Conference of the IEEE Engineering in Medicine and Biology Society—Proceedings, Vol. 16, 1994, pp. 590–591.

[100] J.S. DaPonte, P. Sherman, Classification of ultrasonic image texture by statistical discriminant analysis and neural networks, Comput. Med. Imag. Graphics 15 (1) (1991) 3–9.

[101] S. Yu, L. Guan, S. Brown, Automatic detection of clustered microcalcifications in digitized mammogram films, J. Electron. Imag. 8 (1) (1999) 76–82.

[102] R.M. Nishikawa, M.L. Giger, K. Dol, C.J. Vyborny, R.A. Schmidt, Computer-aided detection of clustered microcalcifications on digital mammograms, Med. Biol. Eng. Comput. 33 (2), March, (1995) 174–178.

[103] S.A. Hojjatoleslami, J. Kittler, Detection of clusters of microcalcification using a K-nearest neighbour classifier, Proceedings of the 1996 IEE Colloquium on Digital Mammography, May 1996, pp. 1–6.

[104] W. Spiesberger, Mammogram inspection by computer, IEEE Trans. Biol. Eng. BMF-26 (4) (1979) 213–219.

[105] J. Marti, J. Batle, X. Cufi, J. Espanol, Microcalcification evaluation in computer assisted diagnosis for digital mammography, Proceedings of the 1999 EE Colloquium on Digital Mammography, 1999, pp. 1–6.

[106] R.M. Nishikawa, Y. Jiang, M.L. Giger, C.J. Vyborny, R.A. Schmidt, R. Bick, Characterization of the mammographic appearance of microcalcifications: applications in computer-aided diagnosis, SPIE Image Process. 1898 (1993) 422–429.

[107] J. Marti, X. Cufi, J. Rgincos, J. Espanol, J. Pont, C. Barcelo, Shape-based features selection for microcalcification evaluation, SPIE 3338 (1998) 1215–1224.

[108] T. Bhangale, U.B. Desai, U. Sharma, An unsupervised scheme for detection of microcalcifications on mammograms, IEEE International Conference on Image Processing, September 10–13, 2000, pp. 184–187.

[109] C.Y. Enderwich, E.M. Tzanakou, Classification of mammographic tissue using shape and texture features, Proceedings of the 19th International Conference-IEEE/EMBS, 1997, pp. 810–813.

[110] R.J. Ferrari, A.C.P.L.F. de Carvalho, P.M.A. Marques, A.F. Frere, Computerized classification of breast lesions: shape and texture analysis using an artificial neural network, Image Process. Appl. (1999) 517–521.

[111] A.P. Dhawan, Y. Chitre, M. Moskowitz, Artificial neural network based classification of mammographic microcalcifications using image structure features, Proc. SPIE 1905 (1993) 820–831.

[112] D. Meersman, P. Scheunders, D.V. Dyck, Classification of microcalcifications using texture-based features, Digital Mammography Nijmegen 1998 (1998) 233–236.

[113] A.P. Dhawan, Y. Chitre, C. Kaiser-Bonasso, M. Moskowita, Analysis of mammographic microcalcifications using grey-level image structure features, IEEE Trans. Med. Imag. 15 (3) (1996) 246–259.

[114] C.S. Lee, J.K. Kim, H.W. Park, Computer-aided diagnostic system for breast cancer by detecting microcalcification, SPIE 3335 (1998) 615–626.

[115] J.S. Geronimo, D.P. Hardin, P.R. Massopust, Fractal functions and wavelet expansions based on several scaling functions, J. Approx. Theory 78 (1994) 373–401.

[116] L. Gagnon, J.M. Lina, B. Goulard, Sharpening enhancement of digitized mammograms with complex symmetric Daubechies wavelets, Annual International Conference of the IEEE Engineering in Medicine and Biology—Proceedings, Vol. 17(1), 1995, pp. 543–544.

[117] F. Rafiee-Rad, H. Soltanina-Zadeh, M. Rahmati, S. Pour-Abdollah, Microcalcification classification in mammograms using multiwavelet features, Proceedings of the 1999 Wavelet Applications in Signal and Image Processing, 1999, pp. 832–841.

[118] H.S. Zadeh, S.P. Nezhad, F.R. Rad, Texture feature extraction methods for microcalcification classification in mammograms, Proc. SPIE 3979 (2000) 982–989.

[119] G.L. Rogova, P.C. Stomper, C. Ke, Microcalcification texture analysis in a hybrid system for computer aided mammography, SPIE 3661 (1999) 1426–1433.

[120] L.P. Cordella, F. Tortorella, M. Vento, Combing experts with different features for classifying clustered microcalcifications in mammograms, Proceedings of 15th International Conference on Patten Recognition, 2000, pp. 324–327.

[121] R.M. Nishlkawa, M.L. Giger, K. Dio, C.J. Vyborny, R.A. Schmidt, Computed-aided detection of clustered microcalcifications: an improved method for grouping detected signals, Med. Phys. 20 (6) (1993) 1661–1666.

[122] A.P. Dhawan, Y. Chitre, C. Bonasso, K. Wheeler, Radial-basis-function based classification of mammographic microcalcifications using texture features, IEEE Proceedings of the 1995 IEEE Engineering in Medicine and Biology 17th Annual Conference and 21st Canadian Medical and Biological Engineering Conference, September 20–23, 1995, pp. 535–536.

[123] T. Chang, C.C. Jay Kuo, Texture analysis and classification with tree-structured wavelet transform, IEEE Trans. Image. Proc. 2 (4) (1993) 429–441.

[124] A. Laine, J. Fan, Texture classification by wavelet packet signatures, IEEE Trans. Pattern Anal. Machine Intel. 15 (11) (1993) 1186–1191.

[125] C.B. Caldwell, S.J. Stapleton, D.W. Holsworth, R.A. Jong, Characterization of mammographic parenchymal pattern by fractal dimension, Phys. Med. Biol. 35 (2) (1990) 235–247.

[126] D.H. Davies, D.R. Dance, C.H. Jones, Automatic detection of microcalcifications in digital mammograms using local area thresholding techniques, SPIE Med. Imag. III: Image Process. 1092 (1989) 153–157.

[127] Dani Kramer, Farzin Aghdasi, Texture analysis techniques for the classification of microcalcifications in digitized mammograms, Proceedings of the 1999 Fifth IEEE AFRICON Conference Electrotechnical Service for Africa, September 28–October 1, 1999, pp. 395–400.

[128] T. Ema, K. Doi, R.M. Nishikawa, Y. Jiang, J. Papaioannou, Image feature analysis and computer-aided diagnosis in mammography: reduction of false-positive clustered microcalcifications using local edge-gradient analysis, Med. Phys. 22 (2) (1995) 161–169.

[129] D. Kramer, F. Aghdasi, Classification of microcalcifications in digitised mammograms using multiscale statistical texture analysis, Proceedings of the South African Symposium on Communications and Signal Processing, September 7–8, 1998, pp. 121–126.

[130] C.M. Kocur, S.K. Gogers, L.R. Myers, T. Burns, M. Kabrisky, J.W. Hoffmeister, K.W. Baver, J.M. Steppe, Using neural networks to select wavelet features for breast cancer diagnosis, IEEE Eng. Med. Biol. 15 (3), May/June, (1996) 95–102.

[131] A.P. Dhawan, Y. Chitre, M. Moskowitz, E. Gruenstein, Classification of mammographic microcalcification and structural features using an artificial neural network, Annual International Conference of the IEEE Engineering in Medicine and Biology Society, Vol. 13(3), 1991, pp. 1105–1106.

[132] Y. Chitre, A.P. Dhawan, M. Moskowitz, Artificial neural network based classification of mammographic microcalcifications using image structure and cluster features, Proceedings of the Annual Conference on Engineering in Medicine and Biology, Vol. 15, 1993, pp. 298–309.

[133] H.S. Zadeh, S.P. Nezhad, F.R. Rad, Shape-based and texture-based feature extraction for classification of microcalcification in mammograms, Proc. SPIE 4322 (2001) 301–310.

[134] Y. Jiang, R.M. Nishikawa, D.E. Wolverton, C.E. Metz, R.A. Schmidt, K. Doi, Computerized classification of malignant and benign clustered microcalcifications in mammograms, Proceedings of 19th International Conference-IEEE/EMBS, October 30–November 2, 1997, pp. 521–523.

[135] A.C. Patrocinio, H. Schiabel, R.H. Benatti, C.E. Goes, F.L.S. Nunes, Investigation of clustered microcalcification features for an automated classifier as part of a mammography CAD scheme, Proceedings of the 22nd Annual EMBS International Conference, July 23–28, 2000, pp. 1203–1205.

[136] M.N. Gurcan, H.P. Chan, B. Sahiner, L. Hadjiiski, N. Petrick, M.A. Helvie, Optimal neural network architecture selection: improvement in computerized detection of microcalcifications, Acad. Radiol. 9 (4) (2002) 420–429.

[137] M.N. Guran, B. Sahiner, H.P. Chan, L. Hadjiiski, N. Petrick, Selection of an optimal neural network architecture for computer-aided detection of microcalcifications—comparison of automated optimization techniques, Med. Phys. 28 (9) (2001) 1937–1948.

[138] B. Sahiner, H.P. Chan, N. Petrick, M.A. Helvie, M.M. Goodsitt, Design of a high-sensitivity classifier based on a genetic algorithm: application to computer-aided diagnosis, Phys. Med. Biol. 43 (1998) 2853–2871.

[139] M.A. Anastasio, H. Yoshida, R. Nagel, R.M. Nishikawa, K. Doi, A genetic algorithm-based method for optimizing the performance of a computer-aided diagnosis scheme for

detection of clustered microcalcifications in mammograms, Med. Phys. 25 (9) (1998) 1613–1620.
[140] H.P. Chan, B. Sahiner, K.L. Lam, Computerized analysis of mammographic microcalcifications in morphological and texture features space, Med. Phys. 25 (1998) 2007–2019.
[141] B. Verma, A neural network based technique to locate and classify microcalcifications in digital mammograms, IEEE International Conference on Neural Networks—Conference Proceedings, Vol. 3, May 4–9, 1998, pp. 1790–1793.
[142] B. Zheng, Y.H. Chang, X.H. Wang, W.F. Good, D. Gur, Application of a Bayesian belief network in a computer-assisted diagnosis scheme for mass detection, SPIE Conference on Image Processing, Vol. 3661, San Diego, CA, February 1999, pp. 1553–1560.
[143] H.D. Li, M. Kallergi, L.P. Clarke, V.K. Jain, R.A. Clark, Markov random field for tumor detection in digital mammography, IEEE Trans. Med. Imag. 14 (3) (1995) 565–576.
[144] L. Zheng, A.K. Chan, An artificial intelligent algorithm for tumor detection in screening mammogram, IEEE Trans. Med. Imag. 20 (17) (2001) 559–567.
[145] F.V. Jensen, An Introduction to Bayesian Network, Springer, New York, NY, 1996.
[146] I.N. Bankman, W.A. Christens-Barry, D.W. Kim, I.N. Weinberg, O.B. Gatewood, W.R. Brody, Automated recognition of microcalcification clusters in mammograms, Proc. SPIE, 1905 (1993).
[147] B. Zhang, Y.H. Chang, X.H. Wang, W.F. Good, Comparison of artificial neural network and Bayesian belief network in a computer-assisted diagnosis scheme for mammography, Proceedings of SPIE—The International Society for Optical Engineering, Vol. 3661, No. II, San Diego, CA, USA, February 22–25, 1999, pp. 1553–1561.
[148] D.C. Edwards, J. Papaioannou, Y. Jiang, M.A. Kupinski, R.M. Nishikawa, Eliminating false-positive microcalcification clusters in a mammography CAD scheme using a Bayesian neural network, Proceedings of SPIE—The International Society for Optical Engineering, Vol. 4322(3), San Diego, CA, USA, February 19–22, 2001, pp. 1954–1960.
[149] M.A. Kupinski, D.C. Edwards, M.L. Giger, C.E. Metz, Ideal observer approximation using Bayesian classification neural networks, IEEE Trans. Med. Imag. 20 (9) (2001).
[150] N.S. Lyer, A. Kandel, M. Schneider, Feature-based fuzzy classification for interpretation of mammograms, Fuzzy Sets and Systems 114 (2) (2000) 271–280.
[151] L.O. Hall, Learned fuzzy rules versus decision trees in classifying microcalcifications in mammograms, Proceedings of SPIE—The International Society for Optical Engineering, Vol. 2761, Orlando, FL, USA, April 1996, pp. 54–61.
[152] K. Woods, M.Y. Sallam, K.W. Bowyer, Evaluating detection algorithms, in: N. Karssemeijer, M. Thijssen, J. Hendriks, L. van Erning (Eds.), Digital Mammography Nijmegen 98, Kluwer Academic Publisher, Amsterdam, 1998, pp. 19–45.
[153] C.E. Metz, ROC methodology in radiologic imaging, Invest. Radiol. 21 (9) (1986) 720–733.
[154] J.A. Swets, ROC analysis applied to the evaluation of medical imaging techniques, Invest. Radiol. 14 (2) (1979) 109–121.
[155] J.L. Maria, G.T. Pablo, S. Miguel, J.M. Arturo, J.V. Juan, Real and simulated clustered microcalcifications in digital mammograms: ROC study of observer performance, Med. Phys. 24 (9) (1997) 1385–1394.
[156] H. Jean, M.C. David, F.B. Charles, P. Zygmunt, J.D. Edward, Preclinical ROC studies of digital stereomammography, IEEE Trans. Med. Imag. 14 (2) (1995) 318–327.
[157] K. Woods, W.B. Kevin, Generating ROC curves for artificial neural networks, IEEE Trans. Med. Imag. 16 (3) (1997) 329–331.
[158] K. Woods, K. Bowyer, A general view of detection algorithms, Proceedings of the Third International Workshop on Digital Mammography, Chicago, 1996, pp. 385–390.
[159] A. Wald, Statistical Decision Functions, Wiley, New York, 1950.
[160] L.B. Lusted, Introduction to Medical Decision Making, Thomas, Springfield, IL, 1968.
[161] L.B. Lusted, Decision-making studies in patient management, N. Engl. J. Med. 284 (1971) 416–424.
[162] L.B. Lusted, Signal detectability and medical decision-making, Science 171 (1971) 1217–1219.
[163] C.E. Metz, P.L. Wang, H.B. Kronman, A new approach for testing the significance of differences between ROC curves measured from correlated data, Proceedings of the Info. Proc. Med. Imaging Eighth Conference, Boston, MA, 1984, pp. 432–445.
[164] J.P. Egan, G.Z. Greenberg, A.I. Schulman, Operating characteristics, signal detectability, and the method of free response, J. Acoust. Soc. Am. 33 (1961) 993–1007.
[165] P.C. Bunch, J.F. Hamilton, G.K. Sanderson, A.H. Simmons, A free-response approach to the measurement and characterization of radiographic observer performance, J. Appl. Photogr. Eng. 4 (1978) 166–171.
[166] D.P. Chakraborty, Free-response methodology: alternate analysis and a new observer performance experiment, Radiology 174 (1990) 873–881.
[167] D.D. Dorfman, E. Alf Jr., Maximum-likelihood estimation of parameters of signal detection theory and determination of confidence intervals: rating method data, J. Math. Psychol. 6 (1969) 487–496.
[168] J. Roehrig, T. Doi, A. Hasegawa, B. Hunt, J. Marshall, H. Romsdahl, A. Schneider, R. Sharbaugh, W. Zhang, Clinical results with R2 Image Checker system, in: N. Karssemeijer, M. Thijssen, J. Hendriks, L. van Erning (Eds.), Digital Mammography Nijmegen 98, Kluwer Academic Publisher, Amsterdam, 1998, pp. 395–400.
[169] www.r2tech.com. R2 Technology Company.
[170] R.M. Nishikawa, M.L. Giger, D.E. Wolverton, R.A. Schimidt, C.E. Comstock, J. Papaioannou, S.A. Collins, K. Doi, Prospective testing of a clinical mammography workstation for CAD: analysis of the first 10,000 cases, in: N. Karssemeijer, M. Thijssen, J. Hendriks, L. van Erning (Eds.), Digital Mammography Nijmegen 98, Kluwer Academic Publisher, Amsterdam, 1998, pp. 401–406.
[171] Elizabeth A. Krupinski, Clinical applications—present and future, in: N. Karssemeijer, M. Thijssen, J. Hendriks, L. van Erning (Eds.), Digital Mammography Nijmegen 98, Kluwer Academic Publisher, Amsterdam, 1998, pp. 47–70.
[172] N. Karssemeijer, J.T.M. Frieling, J.H.C.L. Hendricks, Spatial resolution in digital mammography, Invest Radiol. 24 (1989) 234.
[173] M. Fatemi, L.E. Wold, A. Alizad, J.F. Greenleaf, Vibro-acoustic tissue mammography, IEEE Trans. Med. Imag. 21 (1) (2002) 1–8.

[174] R.J. Grable, S.L. Ponder, N.A. Gkanatsios, W. Dieckmann, P. Oliver, R.H. Wake, Y. Zeng, Optical computed tomography for imaging the breast: first look, Proceedings of SPIE—the International Society for Optical Engineering, Vol. 4082, July 26–28, 2000, pp. 40–45.
[175] H.M. Zonderland, Diagnosis of breast cancer: contribution of US as an adjunct to mammography, Radiology 213 (2) (1999) 413–422.
[176] F. Kasumi, Can microcalcification located within breast carcinomas be detected by ultrasound imaging, Ultrasound Med. Biol. 14 (1) (1988) 175–182.
[177] W.T. Yang, M. Suen, A. Ahuja, C. Meterweli, In vivo demonstration of microcalcification in breast cancer using high resolution ultrasound, Br. J. Radiol. 70 (1997) 685–690.
[178] M. Fatemi, J.F. Greenleaf, Vibro-acoustography system modeling, Era of Hope Proc. 1 (2000) 192.
[179] T.G. McCauley, A. Stewart, M. Stanton, T. Wu, W. Phillips, Three-dimension breast image reconstruction from a limited number of views, Proc. SPIE—Int. Soc. Opt. Eng. 3977 (2000) 384–395.
[180] Jayaram K. Udupa, Gabor T. Herman, 3D Imaging in Medicine, Vols. I and II, CRC Press, Boca Raton, FL, 1991, 1999.
[181] Jayaram K. Udupa, Gabor T. Herman, Medical image reconstruction, processing, visualization, and analysis: the MIPG perspective, IEEE Trans. Med. Imag. 21 (4) (2002) 281–295.
[182] A. Samani, J. Bishop, M.J. Yaffe, D.B. Plewes, Biomechanical 3-D finite element modeling of the human breast using MRI data, IEEE Trans. Med. Imag. 20 (4) (2001) 271–279.
[183] S.P. Bates, S.M. Astley, J.D. Davies, S. Sharp, Three-dimensional reconstruction and shape classification of microcalcification clusters in breast lesions, Proceedings of the Third International Workshop Digital Mammography, Chicago, IL, 1996, pp. 239–244.
[184] A.D.A. Maidment, 3-dimension analysis of breast calcifications, Proceedings of the Third International Workshop Digital Mammography, Chicago, IL, 1996, pp. 245–250.
[185] M. Yam, M. Brady, R. Highnam, C. Behrehbuch, R. English, Y. Kita, Three-dimensional reconstruction of microcalcification clusters from two mammographic view, IEEE Trans. Med. Imag. 20 (6) (2001) 479–489.
[186] H. Tang, T. Zhuang, Ed X. Wu, Realizations of fast 2-D/3-D image filtering and enhancement, IEEE Trans. Med. Imag. 20 (2) (2001) 132–140.

About the Author—HENG-DA CHENG received Ph.D. in Electrical Engineering from Purdue University, West Lafayette, IN, in 1985 (supervisor: K. S. Fu). Currently, he is a Full Professor, Department of Computer Science, and Adjunct Full Professor, Department of Electrical and Computer Engineering, Utah State University. Dr. Cheng is an Adjunct Professor, and Doctorial Supervisor of Harbin Institute of Technology (HIT), and a Guest professor, Remote Sensing Application Institute, Chinese Academy of Sciences, a Guest professor, Wuhan University, a Guest professor, Shantou University and a Visiting professor, Northern Jiaotung University.

Dr. Cheng has published more than 200 technical papers, is the co-editor of the book, *Pattern Recognition*: *Algorithms*, *Architectures and Applications*, and the editor of four conference proceedings. His research interests include: Artificial Intelligence, Computer Vision, Pattern Recognition & Image Processing, Medical Information Processing, Fuzzy Logic, Neural Networks and Genetic Algorithms, Parallel Processing, Parallel Algorithms, and VLSI algorithms and architectures.

Dr. Cheng is the General Chair and Program Chair, the Fifth International Conference on Computer Vision, Pattern Recognition & Image Processing (CVPRIP2003), 2003, and was the General Chair and Program Chair, the Fourth International Conference on Computer Vision, Pattern Recognition & Image Processing (CVPRIP2002), 2002, and General Chair and Program Chair, the Third International Conference on Computer Vision, Pattern Recognition & Image Processing (CVPRIP2000) 2000. He was the General Chair and Program Chair, the First International Workshop on Computer Vision, Pattern Recognition & Image Processing (CVPRIP98), 1998, and was the Program Co-Chair of Vision Interface '90, 1990. He served as a program committee member and session chair for many conferences, and as a reviewer for many scientific journals and conferences.

Dr. Cheng has been listed *Who's Who in the World*, *Who's Who in America*, *Who's Who in Communications and Media*, *Who's Who in Science and Engineering*, *Who's Who in Finance and Industry*, *Men of Achievement*, *2000 Notable American Men*, *International Leaders in Achievement*, *Five Hundred Leaders of Influence*, *International Dictionary of Distinguished Leadership*, etc. He has been appointed as Member of the International Biographical Center Advisory Council, The International Biographical Center, England, and a Member of the Board of Advisors, the American Biographical Institute, USA.

Dr. Cheng is a Senior Member of IEEE society, and a Member of the Association of Computing Machinery. Dr. Cheng is also an Associate Editor of *Pattern Recognition* and an Associate Editor of *Information Sciences*.

About the Author—XIAOPENG CAI received the bachelor of Science degree from the Mathematics Department, Shan Dong University and the Master of Science degree from the Electrical Engineering Department, Shan Tou University, in 1999 and 2002, respectively. Now he is a graduate student of Computer Science Department, Utah State University. His research interests include: pattern recognition, machine learning, signal processing, and image processing, especially on color image and medical image processing.

About the Author—XIAOWEI CHEN received the Bachelor of Science degree from the Department of Applied Physics, Sichuan University, Chengdu, China, in 1992, and the Master of Science degree from the Department of Electrical and Information Engineering, Sichuan University, Chengdu, China, in 1999. Currently he is a MS candidate at the Computer Science Department of Utah State University, Logan, Utah. His research interests are image and signal processing, fuzzy logic, and software engineering.

About the Author—LIMING HU received the Bachelor of Science degree from the Department of Computer Science, in 1995, and the Master of Computer Engineering degree from the Institute of Machine Intelligence, Nankai University, China, in 1998. From 1998 to 2001, he was a software Engineer working on Telecom Software development at Shanghai Bell, Inc. Now he studies Ph.D. program at the Department of Computer Science, Utah State University, Logan, UT. His research interests are image processing and artificial intelligence.

About the Author—XUELING LOU received Bachelor of Science degree from the Department of Computer Science, Wuxi University of Light Industry, Wuxi, China, in 1999. From 1999 to 2001, she was with the Information Technology Department at Seagate Technology Wuxi Co. Ltd. as a software engineer. She studies graduate program in Department of Computer Science, Portland State University since 2002, and will receive Master degree in June, 2003. Her research interests are in Image Processing, Data Mining, Scientific Computing, and Software Engineering.